



HAL
open science

Evaluation of tight-binding DFT performance for the description of organic photochromes properties

Corentin Poidevin, Gwenhaël Duplaix-Rata, Karine Costuas, Arnaud Fihey

► **To cite this version:**

Corentin Poidevin, Gwenhaël Duplaix-Rata, Karine Costuas, Arnaud Fihey. Evaluation of tight-binding DFT performance for the description of organic photochromes properties. *Journal of Chemical Physics*, 2023, 158 (7), pp.074303. 10.1063/5.0133418 . hal-04013814

HAL Id: hal-04013814

<https://hal.science/hal-04013814>

Submitted on 11 May 2023

HAL is a multi-disciplinary open access archive for the deposit and dissemination of scientific research documents, whether they are published or not. The documents may come from teaching and research institutions in France or abroad, or from public or private research centers.

L'archive ouverte pluridisciplinaire **HAL**, est destinée au dépôt et à la diffusion de documents scientifiques de niveau recherche, publiés ou non, émanant des établissements d'enseignement et de recherche français ou étrangers, des laboratoires publics ou privés.

Evaluation of tight-binding DFT performance for the description of organic photochromes properties

Corentin Poidevin,^{*a} Gwenhaël Duplaix-Rata,^a Karine Costuas^a and Arnaud Fihey^{*a}

^a Univ Rennes, CNRS, ISCR (Institut des Sciences Chimiques de Rennes) - UMR 6226, F-35000 Rennes, France. E-mails: corentin.podevin@univ-rennes1.fr, arnaud.fihey@univ-rennes1.fr

Abstract

Photochromic molecules are widely studied and developed for their many potential applications. In this context, it exists a considerable chemical space to explore for the optimization of the required properties and a necessity to understand the impact of their incorporation in devices. To these ends, cheap and reliable computational methods can be powerful tools to steer synthetic developments. As *ab initio* methods remain costly for any extensive studies (in term of size of the system and/or number of molecules), semi-empirical methods like Density Functional Tight-Binding (TB) could offer a good compromise between accuracy computational cost. However, these approaches necessitate benchmarking on the families of compounds of interest. Thus, the aim of the present study is to evaluate the accuracy of several key features calculated with TB methods (DFTB2, DFTB3, GFN2-xTB, and LC-DFTB2) for three sets of photochromic organic molecules, namely azobenzene (AZO), norbornadiene/quadracyclane (NBD/QC) and dithienylethene (DTE) derivatives. The features considered here are the optimized geometries, the difference in energy between the two isomers (ΔE), and of the energies of the first relevant excited states. All the TB results are compared to those obtained with DFT methods and state-of-the-art electronic structure calculation methods: DLPNO-CCSD(T) for ground states and DLPNO-STEOM-CCSD for excited states. Our results show that, overall, DFTB3 is the TB method leading to the best results for the geometries and the ΔE values and can be use alone for these purposes for NBD/QC and DTE derivatives. Single point calculations at the r2SCAN-3c level using TB geometries allow circumvent the deficiencies of the TB methods in the AZO series. For the electronic transition calculation, the range-separated LC-DFTB2 method is the most accurate TB method tested for AZO and NBD/QC derivatives in close agreement with the reference.

1 – Introduction

Molecules able to undergo reversible photoisomerization (photochromes) continue to attract a wide attention for their use in molecular solar thermal storage (MOST), molecular switches, motors or for memory storage.^{1,2,3,4,5,6,7,8,9} To be efficient, these molecules must satisfy several key properties such as: large isomerization quantum yields, significant thermal stability of both isomers, photoisomerization in the range of a photon energy that depends on the application and high energy difference between the two isomers (for energy storage in particular). Designing a molecule to increase the performance of one property can lead to a decrease in performance of another. For instance, for MOST applications, the photoisomerization should occur upon irradiation of photons of energy ranging from 1.5 to 3.5 eV (corresponding the most intense solar radiations reaching the earth surface) while limiting the size of the photochromes to preserve its storage energy density (ideally above 0.3 MJ/kg).^{10,11}

In these contexts, a variety of photochromes have been considered such as azobenzenes,¹² spiroopyrans,¹³ diarylethenes (DTE),¹⁴ or norbornadiene/quadracyclane (NBD/QC).¹⁵ Although many studies have been conducted to find molecular structures with optimized performance, the chemical space to explore remains extremely vast. In this regard, computational methods can offer a valuable approach to narrow this space down by providing insights into structure-properties relationships and thus providing synthetic targets. Additionally, in many applications, the conception of devices necessitates to incorporate or immobilize the photochromic molecules within/on a diversity of support (polymer, carbon nanotube, graphene, metal nanoparticles...). This key step can influence the intrinsic molecular properties.^{16,4,5,3,17} Thus, a fast and cheap quantum theoretical tool appears to be an appealing solution to perform high-throughput computational screening, to study larger systems and account for the environment (neighboring molecules, grafting support, solvent, counterions...) of the active photochrome units in the computational study .

Density functional theory (DFT) methods remain today very costly or even inapplicable for such demanding computational studies. Thus, a good compromise between DFT and classical molecular mechanics methods is to apply quantum semi-empirical methods. Among the wide range of available semi-empirical methods, density functional tight-binding (TB) approaches are particularly interesting tools considering the accuracy of the results versus its computational cost.^{18,19,20,21} These methods rely on the Taylor expansion of DFT energy using a reference electronic density, the sum of neutral atomic densities, and a density difference term

to tackle atomic charge transfer. Methods such as self-consistent-charge density-functional tight-binding (DFTB2)¹⁸ are based on a second order expansion of DFT energy while methods such as DFTB3¹⁹ or GFN2-xTB (XTB2)²⁰ are based on a third order expansion. In this framework, the semi-empirical parameters in DFTB2 and DFTB3 are pair-specific and precomputed using first-principals DFT methods while an element-specific strategy with large fit set is used in the XTB2 method.

While TB methods would in principle allow to explore the photoreaction pathway (reaction barrier but also lifetimes of isomers) with a lower computational cost and to include dynamical effects,²² this remains today remains out of the scope as state of the art wave-function calculations are often necessary to tackle these issues with a satisfying accuracy.²³ To this day the use of TB methods has been mostly limited to ground state and vertical excitations of molecules. These methods have for instance recently been applied by Koerstz *et al.* to study photochromic molecular in a high-throughput computational screening study using Grimme's XTB2²⁰ method in combination with machine learning and DFT in order to screen over 260 billions of substituted dihydroazulene/vinylheptafulvene for MOST applications.²⁴ Additionally, property predictions from DFTB2¹⁸ calculations have been evaluated and compared to those obtained by DFT (using hybrid functionals) for azobenzene and NBD/QC derivatives (10 compounds in each series) by Szabo *et al.*²⁵ They reported a better correlation of the energy differences between the two isomers in the norbornadiene series than in the azobenzene series when comparing DFTB2 to DFT: these values being globally largely overestimated for the NBD/QC and underestimated for the azobenzenes. However, a variation of up to 40 kJ/mol in the calculation of this quantity with various DFT methods is observed, indicating that DFT itself may not be an accurate reference for such properties. To allow a more systematic use of TB methods to design new organic photochromes, there is a need for a more systematic and broad testing of their accuracy for various types of chemical compounds, both for their ground and excited states. The necessary step to do so is to consider whether the accuracy of TB methods is acceptable with respect to highly accurate quantum methods or experimental results. Secondly, the magnitude of error of the calculated physical values associated with the studied properties need to be known. In this context, the identification of the origin of an error in a computational scheme, arising from the geometrical arrangement or from the electronic features, is a precious information.

To this end, we have evaluated the accuracy of several TB methods by focusing on three relevant features of photochromes, *i.e.*, their geometries, the energy difference between their two isomers, and their electronic excitation energies. We have focused our study on three

families of the most popular photochromes which are sufficiently different in their structure to be representative of the chemical space of organic photochromes. The first series contains eleven azobenzene (AZO) derivatives (Figure 1a) in their *trans* and *cis* configuration. AZOs are used in a wide range of applications ranging from material science to biological chemistry and do present appealing features for MOST.^{2,12,26} The second selected series is composed of twelve NBD/QC derivatives also presenting interesting potentiality in MOST (Figure 1b).^{2,27,15,28} The third series is built from sixteen DTE in their open or closed forms. DTE molecular switches are used in molecular electronics or to conceive memory devices (Figure 1c).¹⁴ For each series, we will first focus on assessing the quality of the optimized geometries of the two isomers obtained with TB methods (and at the DFT level for comparison purposes) *versus* state-of-the-art DLPNO-CCSD(T) electronic structure calculations. The errors on the difference in energy between the two forms, ΔE , is the second relevant information which will be considered. In the same way, we will assess the accuracy of the Time Dependent (TD-) DFTB method for the calculation of vertical excitations (UV-Visible absorption), compared to wave-function DLPNO-STEOM-CCSD reference values.

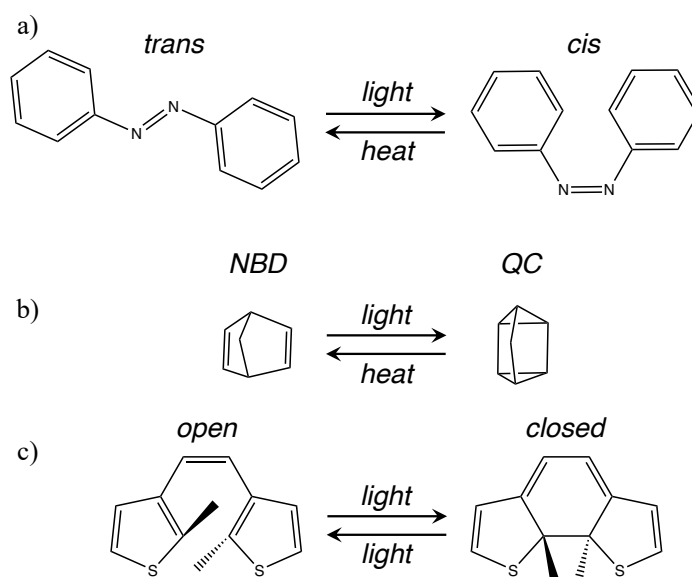


Figure 1. Non substituted molecular structures of the two isomers of a) AZO, b) NBD/QC, c) DTE derivatives.

2 – Methodology and Computational details

Throughout this study, the accuracy of several TB methods are evaluated, namely DTFB2 (*mio* parameters),¹⁸ DFTB3 (*3ob* parameters),¹⁹ GFN2-xTB (XTB2)²⁰ as well as the range separated LC-DFTB2 (*ob2* parameters)²⁹ for the excited states calculations. In all DFTB2 and DFTB3 computations, the effect of Grimme's D3 dispersion corrections³⁰ is also tested. The TB results are also compared to DFT results, using the PBE, B3LYP functionals with D3 corrections and range separated CAM-B3LYP functional for the excited states calculations.^{31,32,33} The recently developed composite method r2SCAN-3c which has been reported to produce accurate geometries and energies at a reduced computational cost is also included in this comparison.³⁴

The geometries of all systems are optimized using the above-mentioned methods (M). The optimized geometry (OG) obtained employing the method M is referred as OG(M), and the calculated total energy of this OG(M) geometry calculated using the method M is labelled as E(M/OG(M)).

To provide a state-of-the art reference, the energy of all the optimized structures are then calculated using the Domain Based Local Pair Natural Orbital Coupled Cluster Singles Doubles and perturbative Triples method (DLPNO-CCSD(T)).³⁵ This method was chosen as the reference in the present study as it leads to results close to those obtained with CCSD(T) which is considered as gold standard for electronic structure calculation of organic molecules. The mean absolute deviation between DLPNO-CCSD(T) with respect to canonical CCSD(T) is reported to be less than 1.7 kJ/mol.³⁶ The OG(M) are compared by calculating their total energies at the DLPNO-CCSD(T) level (reference method) and are denoted thereafter E(CCSD(T)/OG(M)) for compactness. The lowest energy structure at the reference DLPNO-CCSD(T) level among all those obtained for a given isomer is labelled as MinG. By this mean, we assess the quality of all optimized geometries (OG(M)) (of the same isomer) by comparing their DLPNO-CCSD(T) energies (E(CCSD(T)/OG(M))). This also allows estimating the deviation of the structure through their energy difference with the best estimate (E(CCSD(T)/MinG)):

$$E(\text{CCSD(T)/OG(M)}) - E(\text{CCSD(T)/MinG}).$$

In the following, this procedure is used to define the mean errors on the geometries obtained with each method M for each family of compounds.

To complement the energy-based analysis, root-mean-square deviations, using Kabsch algorithm,^{37,38} and mean bond length differences between each structure, OG(M), and the minimum energy structure, MinG, are calculated for both forms of the photochromes. Other

specific bond lengths, angles or dihedral angles are also analyzed depending on the family of compound.

The ΔE value is determined as the difference in total energy between the low-energy and the high-energy isomer. $\Delta E(M/OG(M))$ is thus the ΔE value calculated with the method M for both geometry optimization and energy estimation:

$$\Delta E(M/OG(M)) = E_{\text{low}}(M/OG(M)) - E_{\text{high}}(M/OG(M)).$$

To quantify the errors of each method in the determination of ΔE , two additional ΔE are considered:

$$\Delta E(\text{CCSD(T)/MinG}) = E_{\text{low}}(\text{CCSD(T)/MinG}) - E_{\text{high}}(\text{CCSD(T)/MinG}),$$

which corresponds to the energy difference using DLPNO-CCSD(T) energies at the minimum energy structures, thus representing our best estimate of ΔE .

$$\Delta E(\text{CCSD(T)/OG(M)}) = E_{\text{low}}(\text{CCSD(T)/OG(M)}) - E_{\text{high}}(\text{CCSD(T)/OG(M)}),$$

which corresponds to the ΔE calculated at the DLPNO-CCSD(T) level at the geometries optimized using the method M.

This protocol is applied for all the electronic structure methods mentioned above. The analysis of the results is based on the following differences:

- $\Delta E(M/OG(M)) - \Delta E(\text{CCSD(T)/MinG})$ is the subtraction of the difference in energy between the two isomers (ΔE) while using i) optimized geometries and energies calculated at level M and ii) the energies at the DLPNO-CCSD(T) level with the minimum energy geometries representing the most accurate estimation of ΔE . This gives an estimation of the errors on the ΔE with respect to this reference value.
- $\Delta E(M/OG(M)) - \Delta E(\text{CCSD(T)/OG(M)})$ is the subtraction of the ΔE calculated using the isomers geometries optimized with the method M (OG(M)) and the energies calculated at i) the level M and at ii) the DLPNO-CCSD(T) level. This gives an estimation of the errors on the ΔE restricted to energy consideration only.
- $\Delta E(\text{CCSD(T)/OG(M)}) - \Delta E(\text{CCSD(T)/MinG})$ which represents the difference between the ΔE calculated at the DLPNO-CCSD(T) level with the geometries from the method M and those with the best estimate geometries for each system (MinG). This thus indicates if the structures calculated with the method M could be used to evaluate the ΔE accurately using DLPNO-CCSD(T), in the case where method M do not provide reliable energies.

To complement the assessment of TB accuracy, we evaluate an alternative computational scheme which combines TB geometry optimizations and *low-cost* DFT energy calculations. This approach consists in performing single point calculations at the PBE or r2SCAN-3c level using TB geometries. The accuracy of this approach is then evaluated by the same protocol, i.e. considering the $\Delta E(\text{PBE or r2SCAN-3c/OG(M)}) - \Delta E(\text{CCSD(T)/MinG})$, where again OG(M) refers to the geometries obtained using TB methods.

It has to be noted that the ΔE provided in this study do not include the zero-point vibration, thermal corrections to the enthalpy, nor the entropy as our aim is to compare electronic energies with the gold standard DLPNO-CCSD(T) method for which these corrections are not available. Computed ΔE values were compared to experimental values when available.

The electronic excited states of all the systems are computed using TB methods, more precisely the Time Dependent formalisms, TD-DFTB2³⁹ and its range separated version, TD-LC-DFTB2²⁹ (when needed parameters are available). The DFTB2-D3 geometries are used in both cases. TD-DFT calculations at the PBE and B3LYP levels as well as using the hybrid range separated functional CAM-B3LYP were performed for comparison purpose.³³ Note that TD-DFT calculations with CAM-B3LYP were performed using the B3LYP geometries. The analysis of the TD-TB and TD-DFT electronic excited state accuracy is based on the comparison to the first five excited states calculated at the DLPNO-STEOM-CCSD method.^{40,41,42,43}

Computational details

DLPNO-CCSD(T), DFT and XTB2 calculations were performed using ORCA 5.0 program package.⁴⁴ DFTB2 and DFTB3 calculations were performed using DFTB+ software.⁴⁵ The def2-TZVP basis set⁴⁶ for all PBE, B3LYP and CAM-B3LYP calculations. In addition, the RI (PBE and r2SCAN-3c) or RIJCOSX (B3LYP and CAM-B3LYP) approximations were used to accelerate the SCF procedures.^{47,48} The atom-pairwise dispersion correction with the Becke-Johnson damping scheme (D3BJ) was included except for r2SCAN-3c which already includes dispersion corrections.³⁰ The cc-pVTZ basis set and the *tightPNO* settings were used for all DLPNO-CCSD(T) calculations.^{49,50,51} For the AZO and NBD/QC series, the DLPNO-STEOM-CCSD calculations the def2-TZVP basis set were used. Due to the larger size of the DTE compounds, the def2-TZVP(-f) basis set was preferred in this series. For all geometry

optimizations presented, a vibrational frequency calculation was performed to ensure that the obtained structures were indeed energy minima within each method.

3 – Results and discussion

3.1 – Azobenzene derivatives

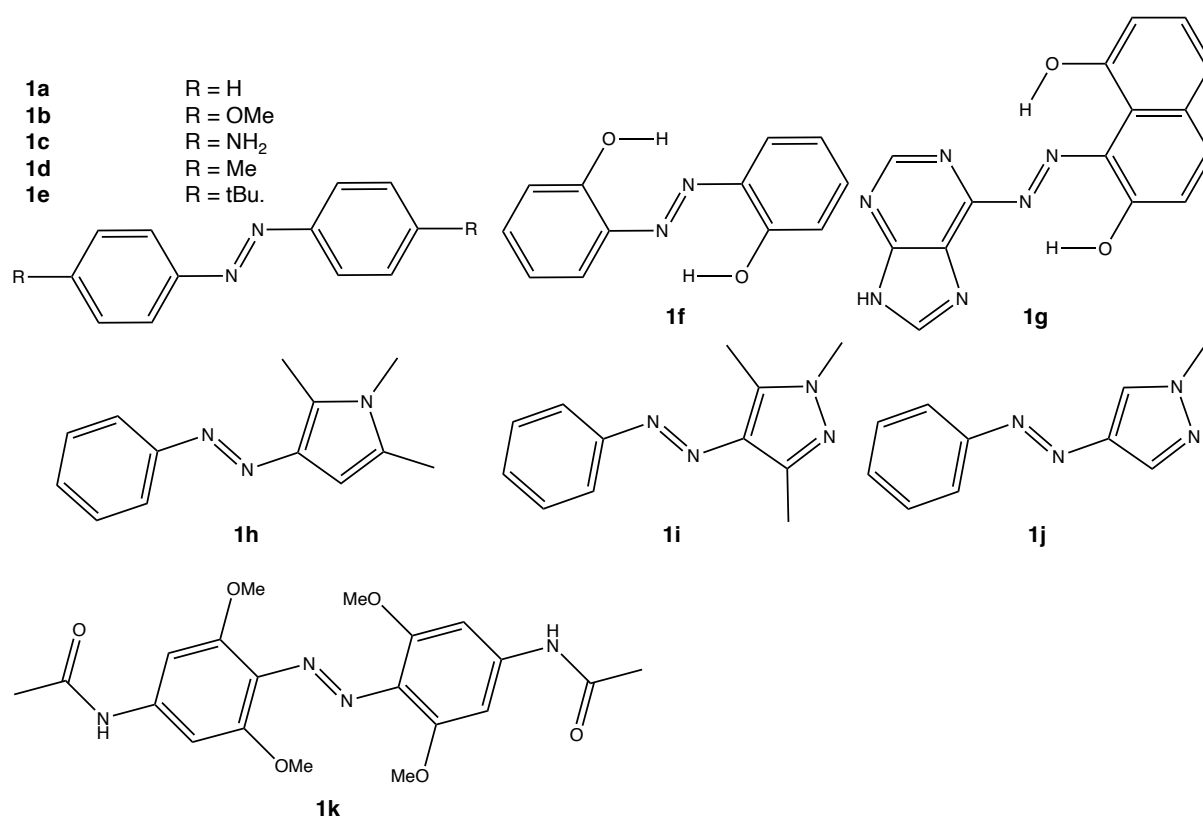


Figure 2. Studied structures for the AZO series.

The set of studied AZO structures is presented in Figure 2. We have selected the pristine azobenzene (**1a**), four para-di-substituted ones (**1b-1e**),⁵² as well as the ortho-di-substituted azobenzene with hydroxyl groups **1f** able to form hydrogen bonds with the nitrogen atoms aiming at stabilizing the trans isomer. **1g** is a parent system of azobenzene for which one benzene is replaced by a OH-substituted naphthalene and the other one by a purine group. Additionally, three arylazopyrazoles (**1h-1j**)⁵³ and a tri-substituted azobenzene (**1k**) were included as they might be of interest for the long half-life of the cis isomer (a few days to about 1000 days).^{53,54}

Geometries

The mean errors and standard deviations in energy of each optimized structure calculated at the DLPNO-CCSD(T) level ($E(\text{CCSD(T)}/\text{OG(M)})$) with respect to the minimum energy structure ($E(\text{CCSD(T)}/\text{MinG})$) are presented in Figure 3. The errors with respect to the lowest structures are homogeneous for each method within the series except for **1g** and **1k**. In these cases, the errors are about 3 to 4 times larger than for the rest of the series with DFTB2(-D3) methods, and about 2 to 3 times larger for DFTB3(-D3) and XTB2. These two molecules are thus removed from the statistical analysis and discussed separately. For **1g**, this discrepancy can arise from H-bonds between the H(-O) and the bridging N being non-negligibly overestimated by TB methods (by 0.3 to 0.2 Å). In the case of **1k**, the *trans* isomer is calculated to be close to planar when optimized with TB methods while steric hindrance (due mostly to the OMe groups) induces significant bending of the structures at the DFT levels. The **1k cis** isomers show the largest deviations of the dihedral angles for all TB methods (Figure 4, bottom right). The methods which are leading to the lowest energy structure for both isomers are B3LYP and r2SCAN-3c followed very closely by PBE. DFTB3 and DFTB3-D3 results are close to those obtained at the PBE level (less than 8 kJ/mol higher) but with a slight increase in the standard deviation. On the other hand, the structures calculated at the DFTB2, DFTB2-D3 and XTB2 levels are about 10 kJ/mol higher in energy than their PBE counterparts. While the structures calculated with DFT methods lead to similar error for both isomers, the *cis* geometries calculated with TB methods deviate more strongly from the reference than the *trans* ones. This difference in error for *cis/trans* remains rather small, less than 3 kJ/mol, with all TB methods.

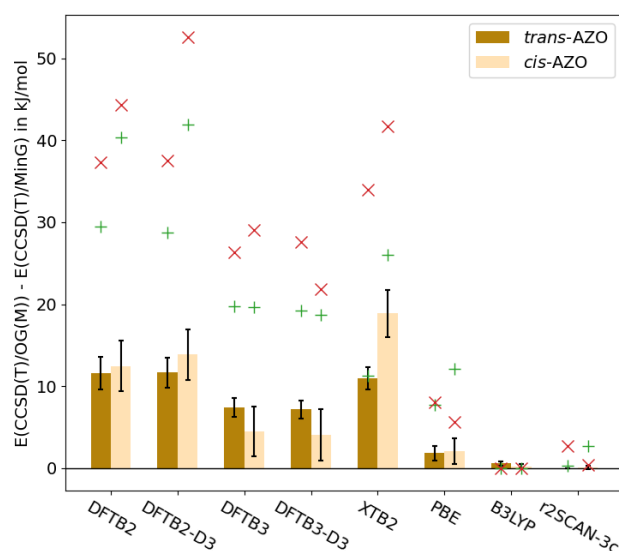
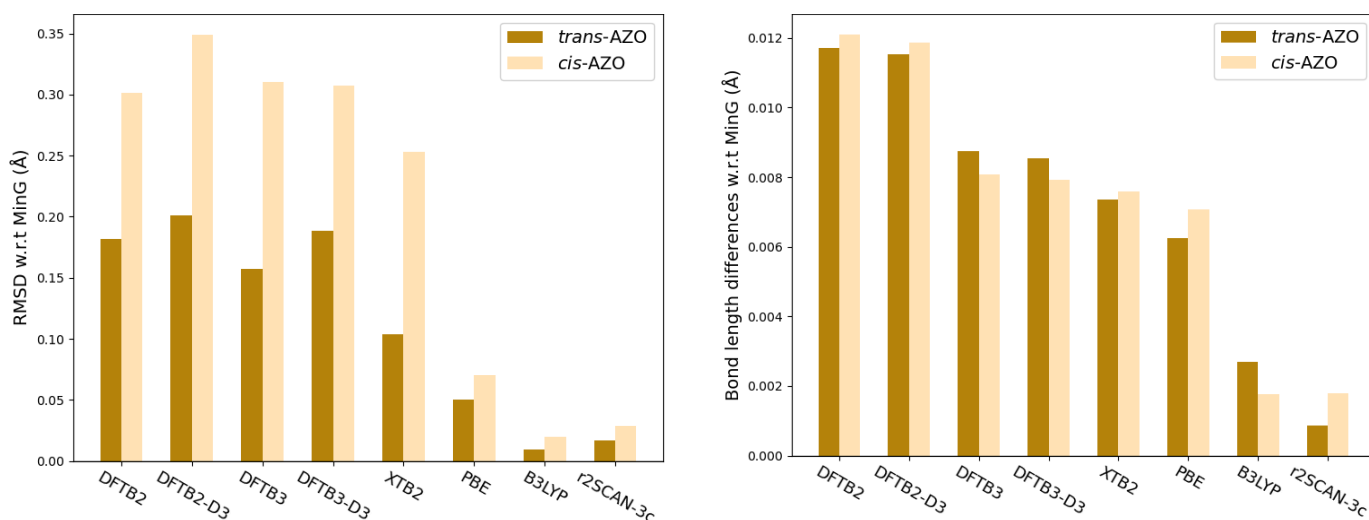


Figure 3. Mean error and standard deviation of $E(\text{CCSD(T)}/\text{OG(M)})$ with respect to $E(\text{CCSD(T)}/\text{MinG})$ for the AZO series. **1g** and **1k** are excluded and their deviations are reported with a green “+” and a red “×”, respectively.

Root mean square deviations (RMSD), bond length differences, N-N bond length differences, and three relevant dihedral angles differences (*cis* isomer, see Figure 5) between each structure and the minimum energy structures are shown in Figure 4. As expected, in most of the cases, the analyses of these geometric parameters are consistent with the results of $E(\text{CCSD(T)}/\text{OG(M)}) - E(\text{CCSD(T)}/\text{MinG})$ (Figure 3). Indeed, the largest deviations in terms of RMSD and bond length differences from MinG geometrical arrangement correspond to higher DLPNO-CCSD(T) energy structures. However, the lower RMSD and the mean bond length differences found for the XTB2 geometries compared to the DFTB3(-D3) results are unexpectedly not leading to lower energy structures. While the energies for the *trans* isomers are comparable for these methods, those of the *cis* isomers are calculated to be much less stable (by about 15 kJ/mol) at the XTB2 level compared to DFTB3(-D3). XTB2 predicts shorter N-N bond lengths in the *cis* isomer than all other tested methods, explaining this deviation.



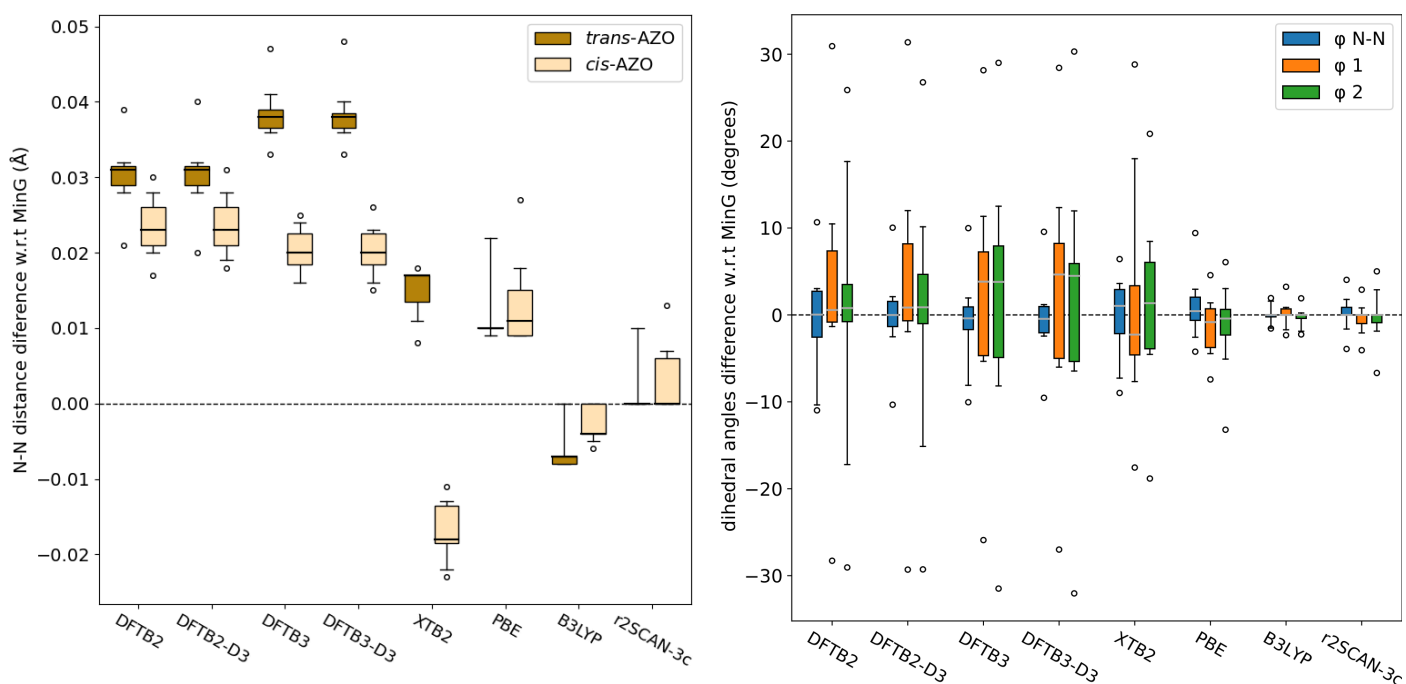


Figure 4. Top left: RMSD between each structure and the minimum energy structure (MinG). Top right: Mean bond length difference between each structure and MinG. Bottom left: N-N bond length difference between each structure and MinG, the lines, boxes, and whiskers denote the median, interquartile range, and the 5th and 95th percentiles, respectively, the circles show the values outside of the latter range (note that these details are transferable to all boxplots in this study). Bottom right: dihedral angles difference between each structure and MinG in the *cis* isomer (see figure 5 for details about the definition of the angles).

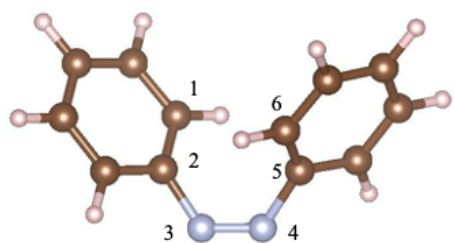


Figure 5. Representation of the investigated dihedral angles: $\varphi_{\text{N-N}} = (1,2,3,4)$ = torsion along the N-N axis, $\varphi_1 = (2,3,4,5)$ and $\varphi_2 = (3,4,5,6)$ = torsions between the phenyl planes and the central unit.

ΔE values

The calculated $\Delta E(\text{CCSD(T)/MinG})$ values for the AZO series are reported in Figure 6 (right). These values correspond to the difference in total energy calculated in vacuum at 0 K and therefore it can only be considered as an approximation of experimental *trans-cis* ΔE (no estimation of the isomerization barrier in this study). For azobenzene (**1a**), This calculated value is quite close to the reported value of ΔE with -49 kJ/mol (Olmsted *et al.*)⁵² vs -51 kJ/mol (this work). Noticeably, the ΔE for **1k** is calculated at +1 kJ/mol, the *cis* isomer being slightly lower

in energy than the *trans* one. The inclusion of the thermal corrections, ZPE, and entropy corrections at the B3LYP level leads to a corrected ΔG of -2 kJ/mol. Experimentally, NMR measurements of DMSO solution of **1k** in the dark reveals that only the *trans* isomer is present. Our calculations suggest that the *cis* isomer is very close in energy at least in vacuum.⁵⁴

The deviation between the ΔE calculated for the geometries optimized at the level M and the one calculated at the DLPNO-CCSD(T) level for the minimum energy structures (MinG) is reported in Figure 6 (left). One can clearly see from the $\Delta E(M/OG(M)) - \Delta E(CCSD(T)/MinG)$ deviations that all TB methods largely underestimate the ΔE in almost all cases, a conclusion that was also recently reported for DFTB2 by Szabo *et al.* for similar AZO compounds.²⁵ The largest deviations from the medians are found for **1g** and **1k** in line with important geometry deviations observed between the MinG and the TB arrangements for those systems. The $\Delta E(CCSD(T)/MinG)$ calculated for **1g** is the largest of the series and present the most underestimated $\Delta E(M/OG(M))$ value with TB methods (about 60 kJ/mol, Figure 6 right). On the other hand, the $\Delta E(M/OG(M))$ of **1k**, possessing the smallest $\Delta E(CCSD(T)/MinG)$, is overestimated by all TB methods. Overall, the largest errors are found when using XTb2, but the distribution of errors for this method is the closest to the median within all TB methods. One can also see that all DFT methods lead to much better $\Delta E(M/OG(M))$ with respect $\Delta E(CCSD(T)/MinG)$.

A similar trend is observed for $\Delta E(M/OG(M)) - \Delta E(CCSD(T)/OG(M))$ deviations. This indicates that the large errors obtained with the TB methods are ultimately not driven by deviations in the geometries, but are mostly induced by a poor evaluation of the relative total energy of the *trans* / *cis* isomers. This conclusion is confirmed by the analysis of $\Delta E(CCSD(T)/OG(M)) - \Delta E(CCSD(T)/MinG)$ deviations: using DLPNO-CCSD(T) to calculate the total energy of the TB structures lead to errors mostly below 10 kJ/mol in all cases. In this framework, DFTB3(-D3) geometries give the best distribution of ΔE . As it was reported for the geometries, the inclusion of D3 corrections do not lead to significant differences in DFTB2 and DFTB3 ΔE values.

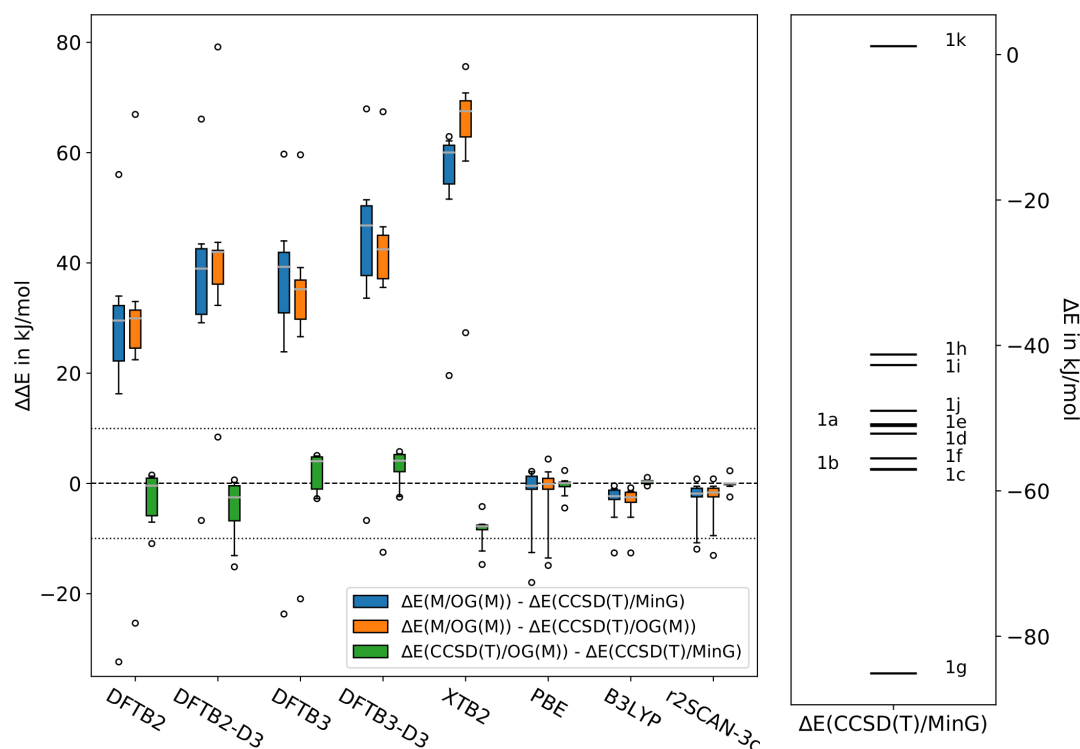


Figure 6. Left: Distribution of $\Delta E(\text{M/OG}(\text{M})) - \Delta E(\text{CCSD}(\text{T})/\text{MinG})$ in blue, $\Delta E(\text{M/OG}(\text{M})) - \Delta E(\text{CCSD}(\text{T})/\text{OG}(\text{M}))$ in orange and $\Delta E(\text{CCSD}(\text{T})/\text{OG}(\text{M})) - \Delta E(\text{CCSD}(\text{T})/\text{MinG})$ in green for the azobenzene series. See figure 4 for details about the boxplots. Right: $\Delta E(\text{CCSD}(\text{T})/\text{MinG})$ corresponding to the reference *trans-cis* energy difference.

The geometries optimized at the TB level can therefore be used to evaluate ΔE using DLPNO-CCSD(T). However, this electronic structure method is much more expensive than any GGA or hybrid functional and prohibitive for large systems (over 100 atoms). As r2SCAN-3c and PBE functionals both allow to access to the electronic structure with a low computational cost, they were also used to conduct single point calculations using the optimized-TB geometries. The resulting $\Delta E(\text{PBE or r2SCAN-3c}/\text{OG}(\text{M})) - \Delta E(\text{PBE or r2SCAN-3c}/\text{OG}(\text{PBE or r2SCAN-3c}))$ and $\Delta E(\text{PBE or r2SCAN-3c}/\text{OG}(\text{M})) - \Delta E(\text{CCSD}(\text{T})/\text{MinG})$ are shown in Figure 7. The distribution of errors are below 10 kJ/mol in all cases. Within this mixed calculation scheme, the best results are found for DFTB3(-D3) geometries when using r2SCAN-3c for the electronic structure calculations.

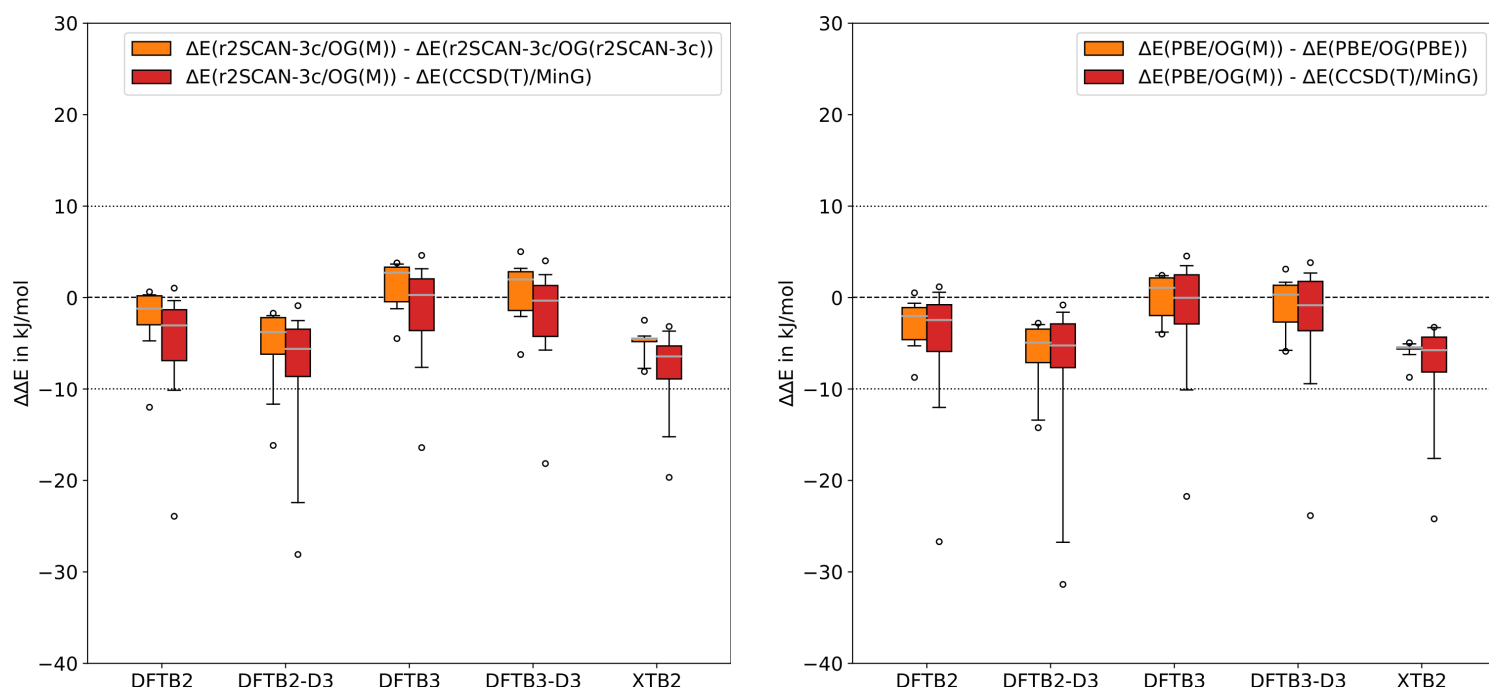


Figure 7. Left: Distribution of the errors of $\Delta E(\text{r2SCAN-3c/OG(M)}) - \Delta E(\text{r2SCAN-3c/OG(r2SCAN-3c)})$ and $\Delta E(\text{r2SCAN-3c/OG(M)}) - \Delta E(\text{CCSD(T)/MinG})$ for the AZO series. Right: Distribution of the errors of $\Delta E(\text{PBE/OG(M)}) - \Delta E(\text{PBE/OG(PBE)})$ and $\Delta E(\text{PBE/OG(M)}) - \Delta E(\text{CCSD(T)/MinG})$ for the AZO series. See figure 4 for details about the boxplots.

The first relevant vertical electronic excitation of both isomers of AZOs were computed with the different methods. Energies and the oscillator strength of the excited state corresponding to the first maximum absorption (FMA) obtained with TD-DFTB2, TD-LC-DFTB2, PBE, B3LYP, CAM-B3LYP and DLPNO-STEOM-CCSD are shown in Figure 8 (the first five excited states are compared in Figure S1). For the *trans* isomer, this excited state corresponds to the first $\pi\text{-}\pi^*$ transition and for the *cis* isomer it corresponds to a $n\text{-}\pi^*$ transition. CAM-B3LYP is the DFT functional which leads to excited states that are in average in best agreement with DLPNO-STEOM-CCSD as reported in Table 1. In almost all cases, the energies and the oscillator strengths of the excited states calculated at the DFTB2 level are very close to those obtained at the PBE level. LC-DFTB2 energies and oscillator strengths are very close (but slightly higher) to those calculated with CAM-B3LYP, except for the first excited state of the *trans* isomer which corresponds to a dark $n\text{-}\pi^*$ transition (see SI). Humeniuk *et al.* already showed that the energies of the $n\text{-}\pi^*$ states were underestimated at the LC-DFTB2 level compared to the well described $\pi\text{-}\pi^*$ states.⁵⁵

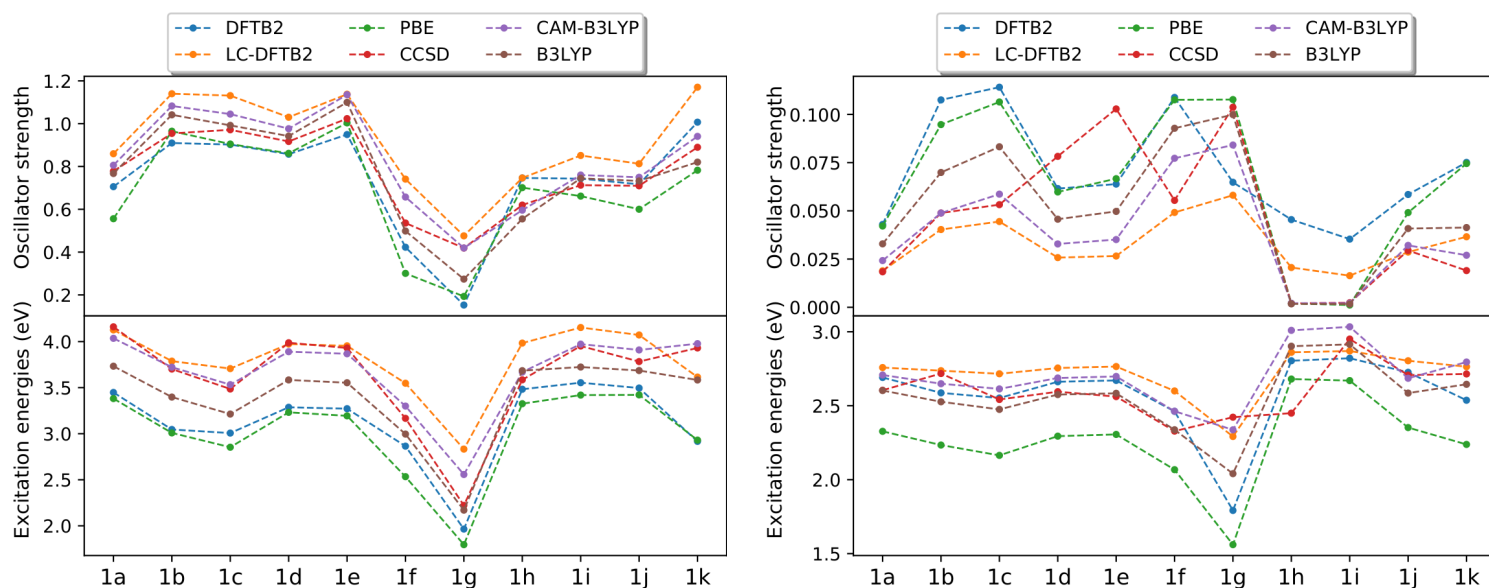


Figure 8. First intense singlet excited state energies and oscillator strength of the AZO series in the *trans* (left) and *cis* (right) isomer form calculated using DFTB2, LC-DFTB2, PBE, B3LYP, CAM-B3LYP, and STEOM-DLPNO-CCSD (see Methodology section for details).

Table 1. Mean absolute errors on energies (eV) and oscillator strength of the first maximum in absorption (FMA) with respect to the one calculated with STEOM-DLPNO-CCSD for the AZO series.

	DFTB2		LC-DFTB2		PBE		B3LYP		CAM-B3LYP	
	<i>trans</i>	<i>cis</i>								
FMA	0.51	0.17	0.23	0.16	0.62	0.38	0.25	0.12	0.10	0.13
<i>f</i>	0.08	0.04	0.14	0.02	0.11	0.03	0.05	0.02	0.06	0.02

As a more specific illustration, the simulated UV-visible spectra of the *trans* and *cis* isomers of **1a** are shown in Figure 9. The excited states description (principal monoexcitations, electronic excitation energy and oscillator strength) as well as the relevant molecular orbitals are given in the SI (Table S5 and S6). These results reveal that the nature of the first excited states of azobenzene are identical for all levels of theory used here. A recent experimental study on the absorption properties of the *trans* and *cis* azobenzene gives an absorption maximum in methanol at 3.96 eV and 4.43 eV, respectively.⁵⁶ When accounting for a bathochromic shift due to the solvent, these values are in line with LC-DFTB2, CAM-B3LYP and DLPNO-STEOM-CCSD results. This makes LC-DFTB2 the most accurate TB method to describe vertical electronic excitations in AZO derivatives.

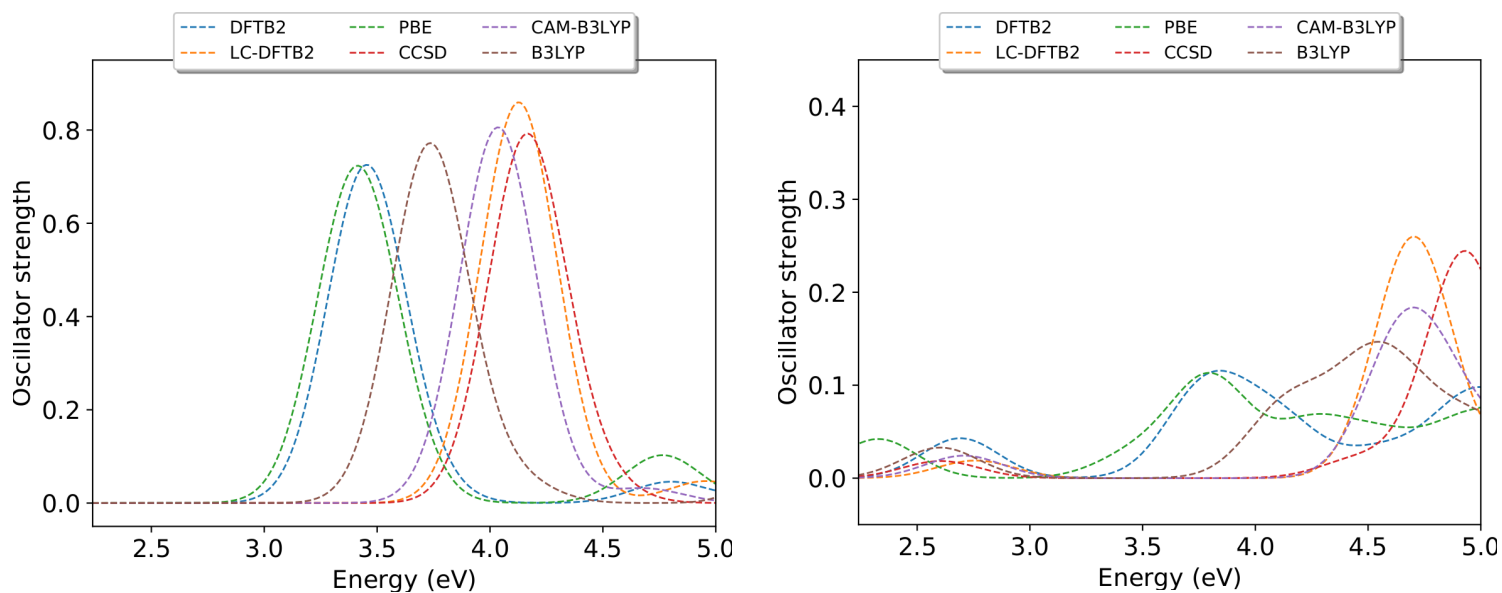


Figure 9. Simulated UV-Visible spectra of the *trans* (left) and *cis* (right) isomers of **1a** calculated using DFTB2, LC-DFTB2, PBE, B3LYP, CAM-B3LYP, and STEOM-DLPNO-CCSD (see Methodology section for details, convolution with gaussian functions with a full-width at half-maximum of 0.2 eV).

The study of AZO derivatives using TB methods can be summarize as follows:

- The best geometries are obtained with DFTB3(-D3) among the set of studied TB methods,
- All tested TB methods fail at predicting satisfyingly ΔE (large underestimation),
- However, combination of TB methods for geometry optimization (DFTB3(-D3)) and single point calculations at relatively low-cost DFT levels (PBE and r2SCAN-3c) lead to a good estimation of the ΔE and appears as an appealing alternative,
- LC-DFTB2 gives remarkably good results for the calculation of electronic excited states and can be considered as the TB method of choice for AZO derivatives optical properties.

3.3 – NBD/QC derivatives

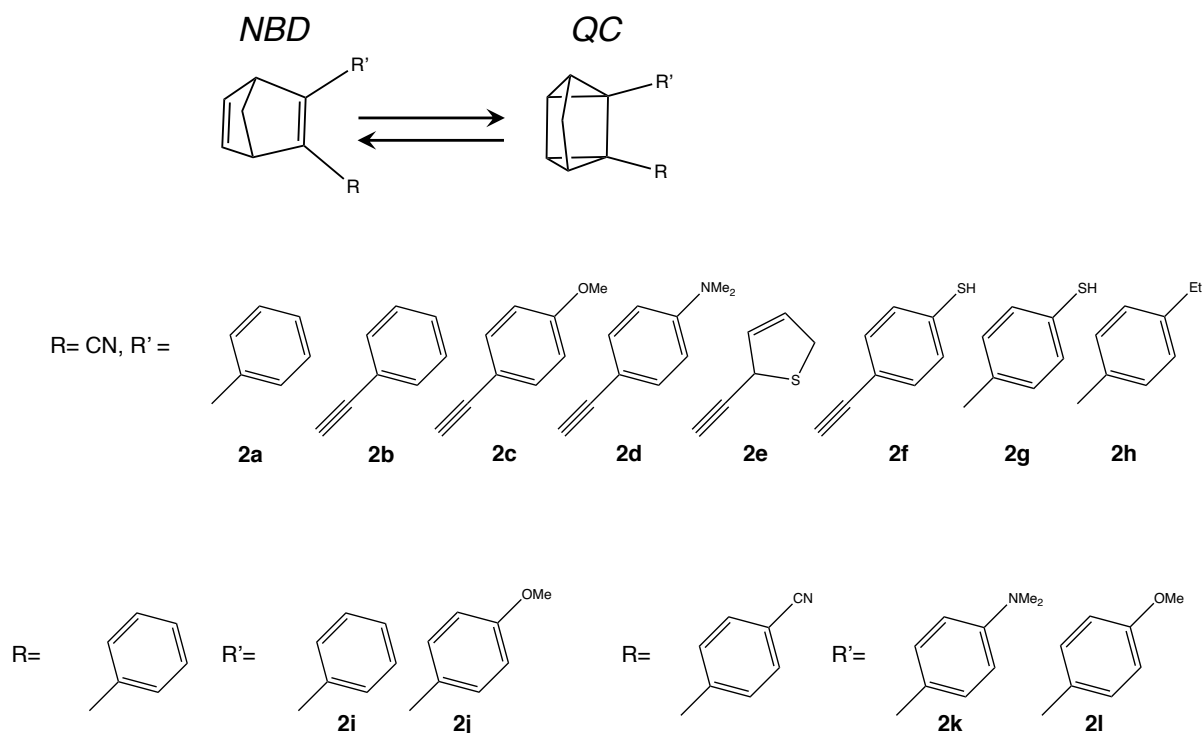


Figure 10. Studied structures for the NBD/QC series.

The set of NBD/QC structures studied here is presented in Figure 10 and were developed by the group of Moth-Poulsen. Eight of these structures (**2a-2e**) possess a cyano group in R position and different substitutions in R' position: a phenyl (**2a**), a phenylalkynyl (**2b**), a p-methoxyphenyl (**2c**), a p-dimethylaminophenyl (**2d**) and a 2-thiophenyl (**2e**).²⁷ Three additional R' substitutions were added two complete the set with a p-thiophenol-alkynyl (**2f**), a p-thiophenol (**2g**) and a p-ethylphenyl (**2h**) as R' substituents. The last four compounds of the series (**2i-2l**) contain a phenyl or a cyanophenyl in R, and phenyl, aminophenyl and methoxyphenyl in R' position.⁵⁵ The experimental energy storage of **2a** and **2d** were found to be -122 kJ/mol and -103 kJ/mol, respectively, which is about twice as large as what is observed in azobenzene derivatives.²⁷

The mean errors and standard deviations along this set of molecules calculated at the DLPNO-CCSD(T) level (E(CCSD(T)/OG(M)) with respect to the minimum energy structures (E(CCSD(T)/Min) are presented in Figure 11. As for the AZO series, the DFT methods lead to the lowest energy structures for both forms with the least deviation obtained with B3LYP and r2SCAN-3c followed very closely by PBE. Here, DFTB3 and DFTB3-D3 results are only 2 kJ/mol higher in energy for the NBD and 4 kJ/mol higher for the QC. The energies of the structures calculated at the DFTB2, DFTB2-D3 and XTB2 are comparable and about 11 kJ/mol higher than E(CCSD(T)/MinG). The errors with respect to the lowest structures (MinG) are of

similar magnitude for both isomers at a given method. The variations are similar within the series, contrarily to the AZO series in which large deviations were found for **1g** and **1k**. This can be explained by the fact that this NBD/QC series is chemically more homogeneous. The accuracy of the structures obtained for the NBD and the QC forms are similar, with a 2 kJ/mol change in error for TB methods and with a 1 kJ/mol change for DFT methods.

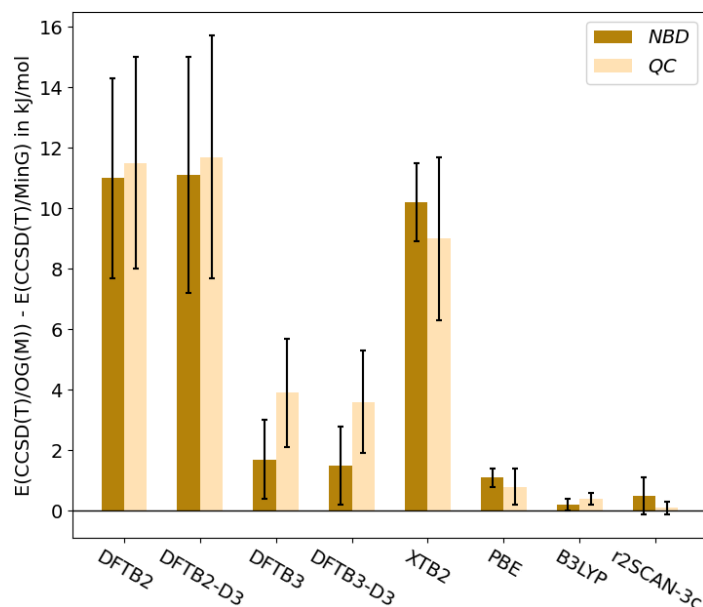


Figure 11. Mean error and standard deviation of $E(\text{CCSD(T)/OG(M)})$ with respect to $E(\text{CCSD(T)/MinG})$ for the NBD/QC series.

RMSD, mean bond length differences (especially the difference in the C-C bond involved in the closing from NBD to QC), and a dihedral angle (φ , represented in Figure 13) difference between each structure and the minimum energy structures are shown in Figure 12. All TB methods show RMSDs in the QC form about three times higher than the ones in the NBD forms. This can be explained by the difference observed on the values of the dihedral angle compared to that of the minimum energy structures in the QC form. Indeed, this dihedral angle, between the QG core and phenyl moiety, is systematically calculated to be smaller for all TB methods compared to DFT methods. Overall, the mean bond length differences follow nicely the mean errors observed for the energies (see Figure 11). Interestingly, while the energy deviations for structures calculated at the PBE level are very small, the RMSD, mean bond length differences, and to a lesser extent, the dihedral angle differences are close to the ones obtained using TB methods. An accurate description of the closing C-C bonds is thus a key factor to obtain low-energy structure.

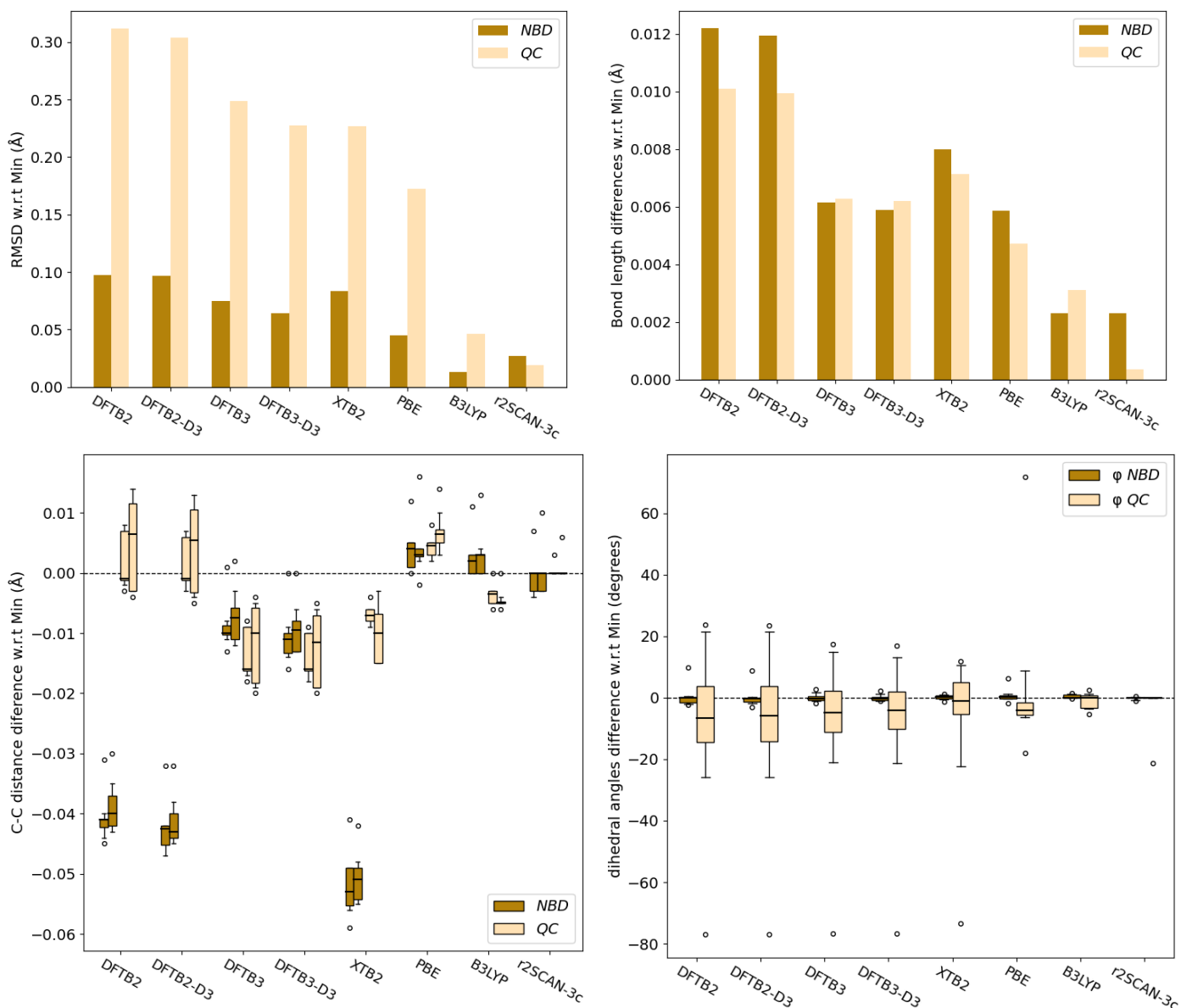


Figure 12. Top left: RMSD of chosen geometric parameters between each structure and the minimum energy structure (MinG). Top right: Mean bond length difference between each structure and MinG. Bottom left: the two closing C-C bond length differences between each structure and MinG. Bottom right: dihedral angle difference between each structure and MinG (see figure 15 for details about the definition of the angles). See figure 4 for details about the boxplots.

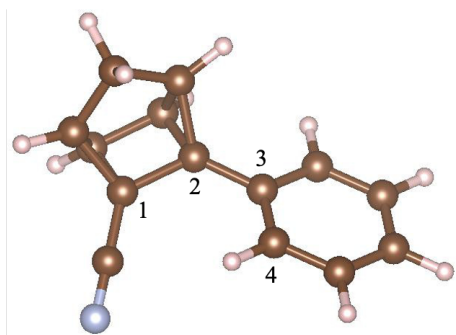


Figure 13. Illustration of the dihedral angle: φ corresponds to the dihedral angle between atoms 1, 2, 3 and 4 (atoms 3 and 4 always from the phenyl unit, even when a CC triple bond is present in group R').

The calculated $\Delta E(\text{CCSD(T)/MinG})$ values for the NBD/QC series are reported in Figure 14. The computed ΔE are in good agreement with the available experimental ΔG for **2a** and **2d**, with -108 vs -122 kJ/mol and -111 vs -103 kJ/mol, respectively. The comparison of the calculated ΔE using each electronic structure methods (M) with respect to the ΔE calculated at the DLPNO-CCSD(T) level using both the structures obtained with method M and the minimum energy structure (MinG) is reported in Figure 14 (left). From $\Delta E(\text{M/OG(M)}) - \Delta E(\text{CCSD(T)/MinG})$ values, one can see that DFTB2 largely overestimates ΔE and that XTB2 largely underestimates it. On the other hand, the ΔE calculated at the DFTB3(-D3) levels are remarkably close to the $\Delta E(\text{CCSD(T)/MinG})$ and even outperform the PBE, B3LYP and r2SCAN-3c.

As for the AZO series, the same trend is observed for $\Delta E(\text{M/OG(M)}) - \Delta E(\text{CCSD(T)/OG(M)})$ for all methods. This indicates that the large errors obtained using DFTB2(-D3) or XTB2 is not primarily due to deviations in the geometries calculated with these methods rather to the poor evaluation of the NBD-QC relative energies as confirmed by the $\Delta E(\text{CCSD(T)/OG(M)}) - \Delta E(\text{CCSD(T)/MinG})$ values. This demonstrate that using the TB geometries with DLPNO-CCSD(T) single points lead to homogeneous deviations of the ΔE values, below the 10 kJ/mol error. This is observed for all tested TB methods including DFTB3(-D3). As in the AZO series, for DFTB2 and DFTB3, the inclusion of D3 corrections do not lead to significant differences.

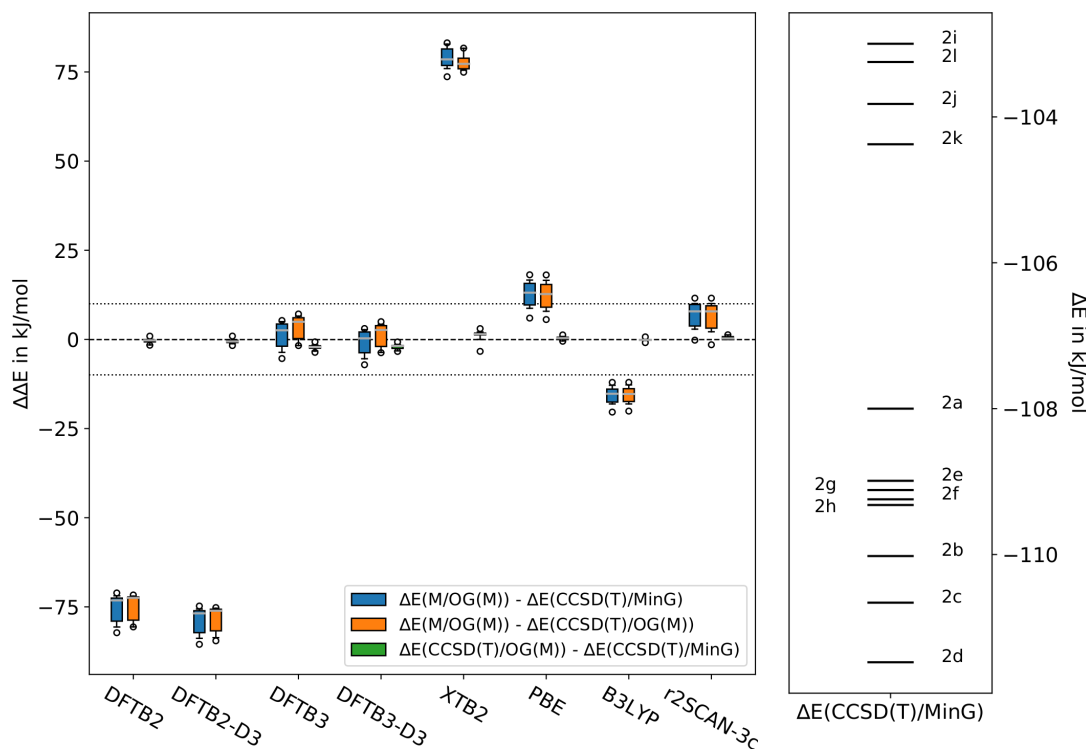


Figure 14. Left: Distribution of the errors of $\Delta E(\text{M}/\text{OG}(\text{M})) - \Delta E(\text{CCSD}(\text{T})/\text{MinG})$ in blue, $\Delta E(\text{M}/\text{OG}(\text{M})) - \Delta E(\text{CCSD}(\text{T})/\text{OG}(\text{M}))$ in orange and $\Delta E(\text{CCSD}(\text{T})/\text{OG}(\text{M})) - \Delta E(\text{CCSD}(\text{T})/\text{MinG})$ in green for the NBD/QC series. See figure 4 for details about the boxplots. Right: $\Delta E(\text{CCSD}(\text{T})/\text{MinG})$ corresponding to the electronic energy of the NBD form minus that of the QC form.

Interestingly, using the DFTB3(-D3) method both to optimize the geometries and to calculate ΔE returns satisfying results in the NBD/QC series which was not the case in the AZO molecules. This is not true for DFTB2(-D3) and XTB2 methods, though their geometries can be used for an electronic structure calculation at the DLPNO-CCSD(T) level. As for the AZO series, we thus computed $\Delta E(\text{PBE or r2SCAN-3c}/\text{OG}(\text{M})) - \Delta E(\text{PBE or r2SCAN-3c}/\text{OG}(\text{PBE or r2SCAN-3c}))$ and $\Delta E(\text{PBE or r2SCAN-3c}/\text{OG}(\text{M})) - \Delta E(\text{CCSD}(\text{T})/\text{MinG})$ for all TB methods (Figure 15). Overall, the best energy results are obtained when using r2SCAN-3c to calculate the energy (median error of less than 10 kJ/mol) after a TB geometry optimization. DFTB3(-D3) is the best TB choice for optimizing the NBD/QC geometries as in the AZO series.

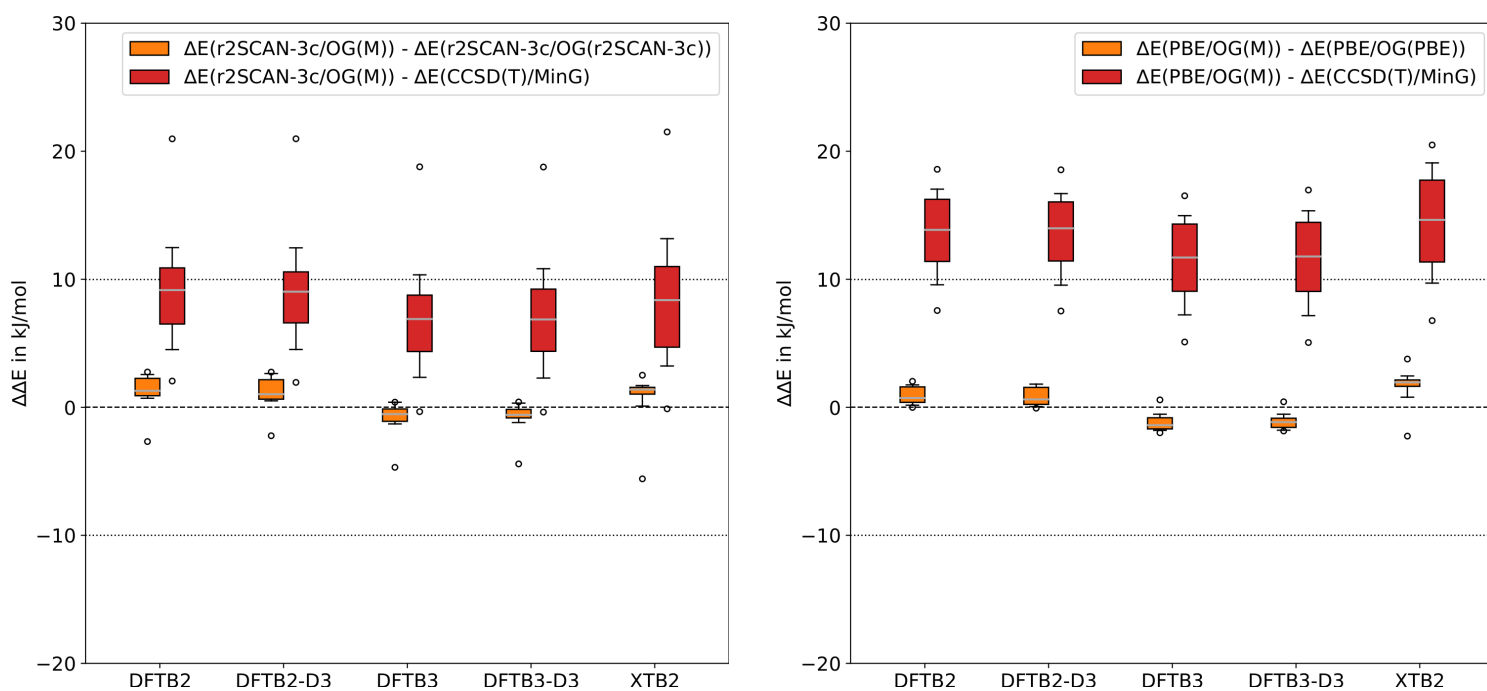


Figure 15. Left: Distribution of the errors of $\Delta E(\text{r2SCAN-3c/OG(M)}) - \Delta E(\text{r2SCAN-3c/OG(r2SCAN-3c)})$ and $\Delta E(\text{r2SCAN-3c/OG(M)}) - \Delta E(\text{CCSD(T)/MinG})$ for the NBD/QC series. Right: Distribution of the errors of $\Delta E(\text{PBE/OG(M)}) - \Delta E(\text{PBE/OG(PBE)})$ and $\Delta E(\text{PBE/OG(M)}) - \Delta E(\text{CCSD(T)/MinG})$ for the NBD/QC series. See figure 4 for details about the boxplots.

Energies and oscillator strengths of the first intense electronic excitation were computed at the TD-DFTB2, TD-LC-DFTB2, PBE, B3LYP, CAM-B3LYP and DLPNO-STEOM-CCSD levels for both isomers. The main results are gathered in Figure 16 (the first five excited states are compared in Figure S2). Note that **2e**, **2f** and **2g** could not be investigated with LC-DFTB2 due to the absence of parameters for sulfur. The first excited state of all NBD molecules corresponds to a $\pi\text{-}\pi^*$ transition including the four carbon atoms that are involved in the NBD to QC isomerization, regardless of the method. These excitations are largely dominated by a HOMO-LUMO transitions. In the case of the QC isomers, the electronic excitation that is mainly described by the HOMO-LUMO transition also corresponds to a $\pi\text{-}\pi^*$ transition. It has to be noted that it is not necessarily the first excited state (see Table S3, S7 and S8). As in the AZO series, CAM-B3LYP is the functional leading to excited states that are in average in best agreement with DLPNO-STEOM-CCSD as presented in Table 2. LC-DFTB2 calculations lead to excited state energies and oscillator strengths relatively close to those calculated at the DLPNO-STEOM-CCSD and CAM-B3LYP levels. As in the AZO series, the energies of the electronic excited states calculated at the DFTB2 level are very close to those obtained at the PBE level.

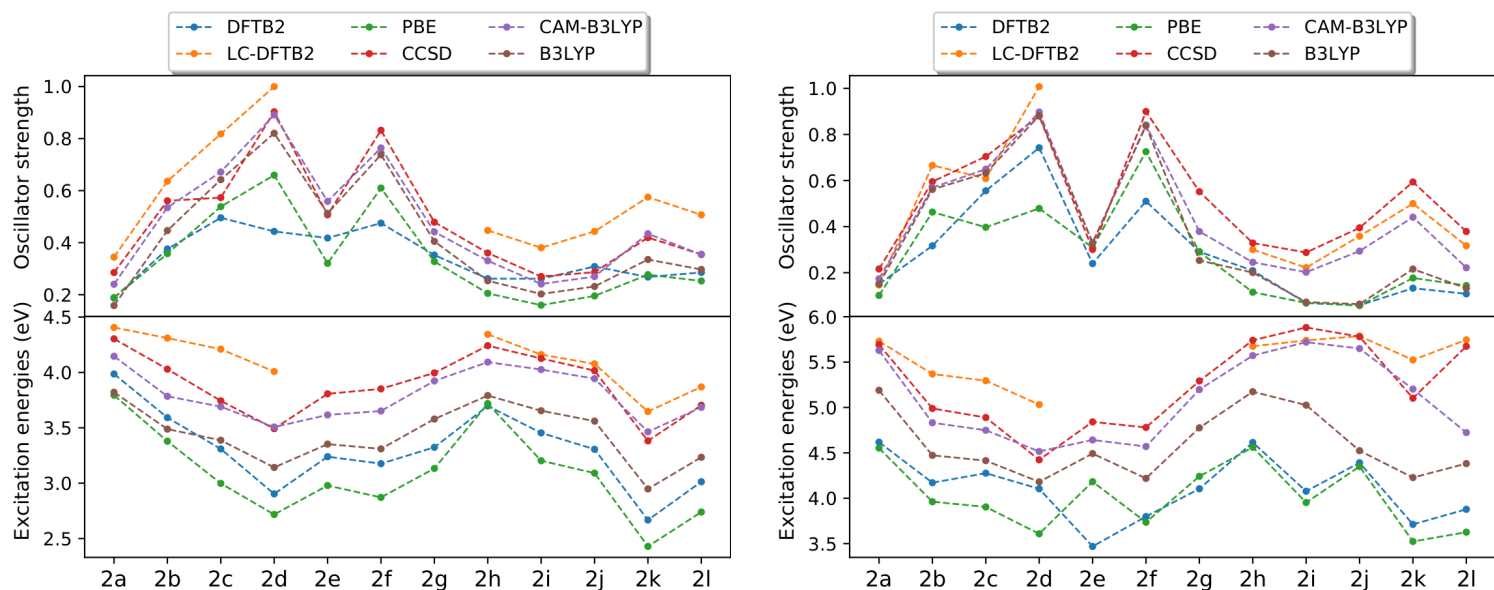


Figure 16. First intense singlet excited state energies and associated oscillator strengths of the NBD/QC series in the NBD (left) and QC (right) forms calculated using DFTB2, LC-DFTB2, PBE, B3LYP, CAM-B3LYP, and STEOM-DLPNO-CCSD (see Methodology section for details).

Table 2. Mean absolute errors (eV) of the first maximum absorption (FMA) with respect to STEOM-DLPNO-CCSD one at the B3LYP geometries for the NBD/QC series.

	DFTB2		LC-DFTB2		PBE		B3LYP		CAM-B3LYP	
	NBD	QC	NBD	QC	NBD	QC	NBD	QC	NBD	QC
FMA	0.59	1.16	0.22	0.24	0.80	1.24	0.45	0.67	0.11	0.21
f	0.15	0.23	0.13	0.07	0.14	0.23	0.08	0.16	0.04	0.08

We illustrate these performances by analyzing the simulated UV-visible spectra of the NBD and QC form of **2d** which are shown in Figure 17. Additionally, the excited state descriptions, principal monoexcitations, excitation energy and oscillator strength) as well as the relevant molecular orbitals are presented in Table S7 and S8. The nature of the first excited state of **2d** NBD is of the same nature for all the level of theory used and it is also the state responsible for the first intense absorption peak. However, the order of the other excited states depends mostly on the type of method used, *i.e.* range separated or non-range separated (see Table S7 and S8). For **2d** QC, the electronic excitation which is described by a HOMO to LUMO transition is the maximum absorption peak and either the first or the second electronic excitation depending on the method. Experimentally, the first maximum absorption band for the NBD form of **2d** in toluene is measured at ca. 3.1 eV and at ca. 4.1 eV for the QC form.²⁷

When accounting for a bathochromic shift due to the solvent, these values are in line with CAM-B3LYP and DLPNO-STEOM-CCSD results. LC-DFTB2 overestimates this excitation energy in both cases. As it can be seen in Figure S2, this overestimation is systematic along the series of NBD/QC, but more or less pronounced depending on the compound.

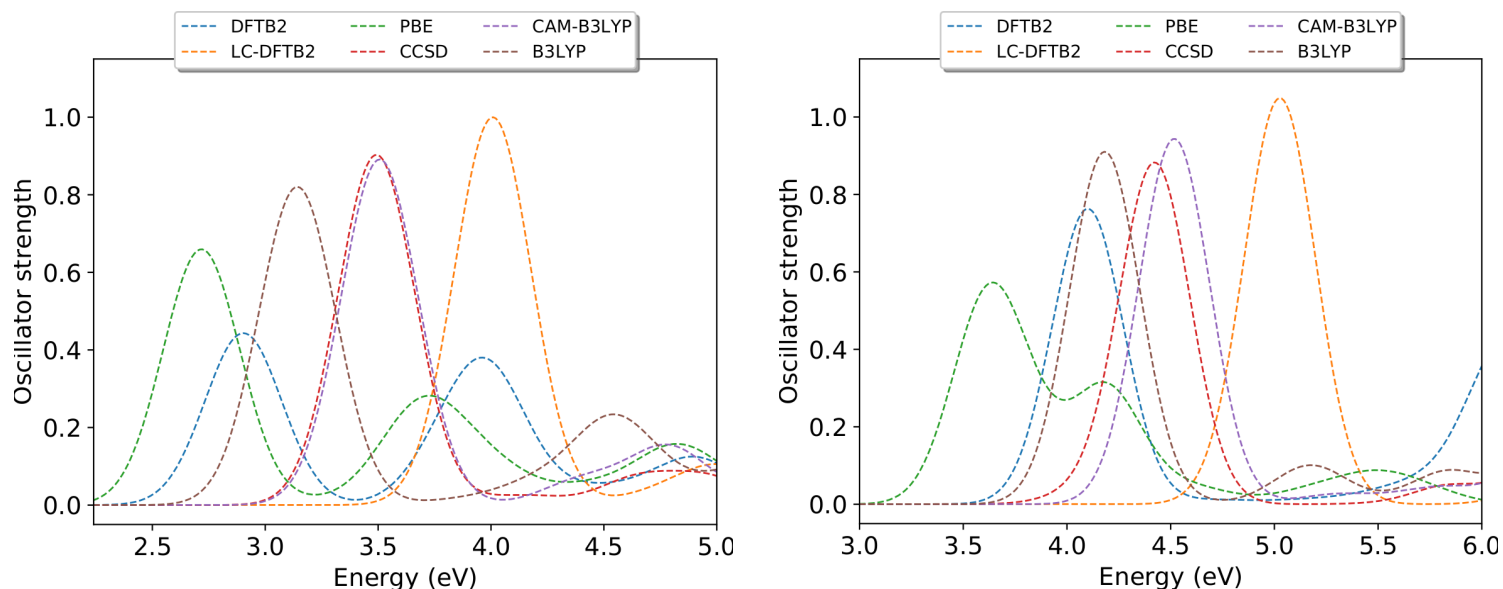


Figure 17. Simulated UV-Visible spectra of the trans (left) and cis (right) isomers of 2d calculated using DFTB2, LC-DFTB2, PBE, B3LYP, CAM-B3LYP, and DLPNO-STEOM-CCSD (see Methodology section for details, convolution with gaussian functions with a full-width at half-maximum of 0.2 eV).

From this investigation of TB performances to tackle norbornadiene/quadricyclane derivatives, the main conclusions are:

- The best geometries are obtained with DFTB3(-D3),
- DFTB2 and XTB2 fail at predicting ΔE (large overestimation and underestimation, respectively),
- DFTB3 lead to very good prediction of ΔE which allows to perform TB-only investigations (DFTB3 / DFTB3(-D3))
- As for the AZO series, single point calculations at DFT levels using TB methods geometries lead to a good estimation of the ΔE especially using r2SCAN-3c.
- LC-DFTB2 gives better estimation of excitation energies compared to DFTB2 but with larger errors than for the AZO derivatives (overestimation of excitation energies).

3.4 – DTE derivatives

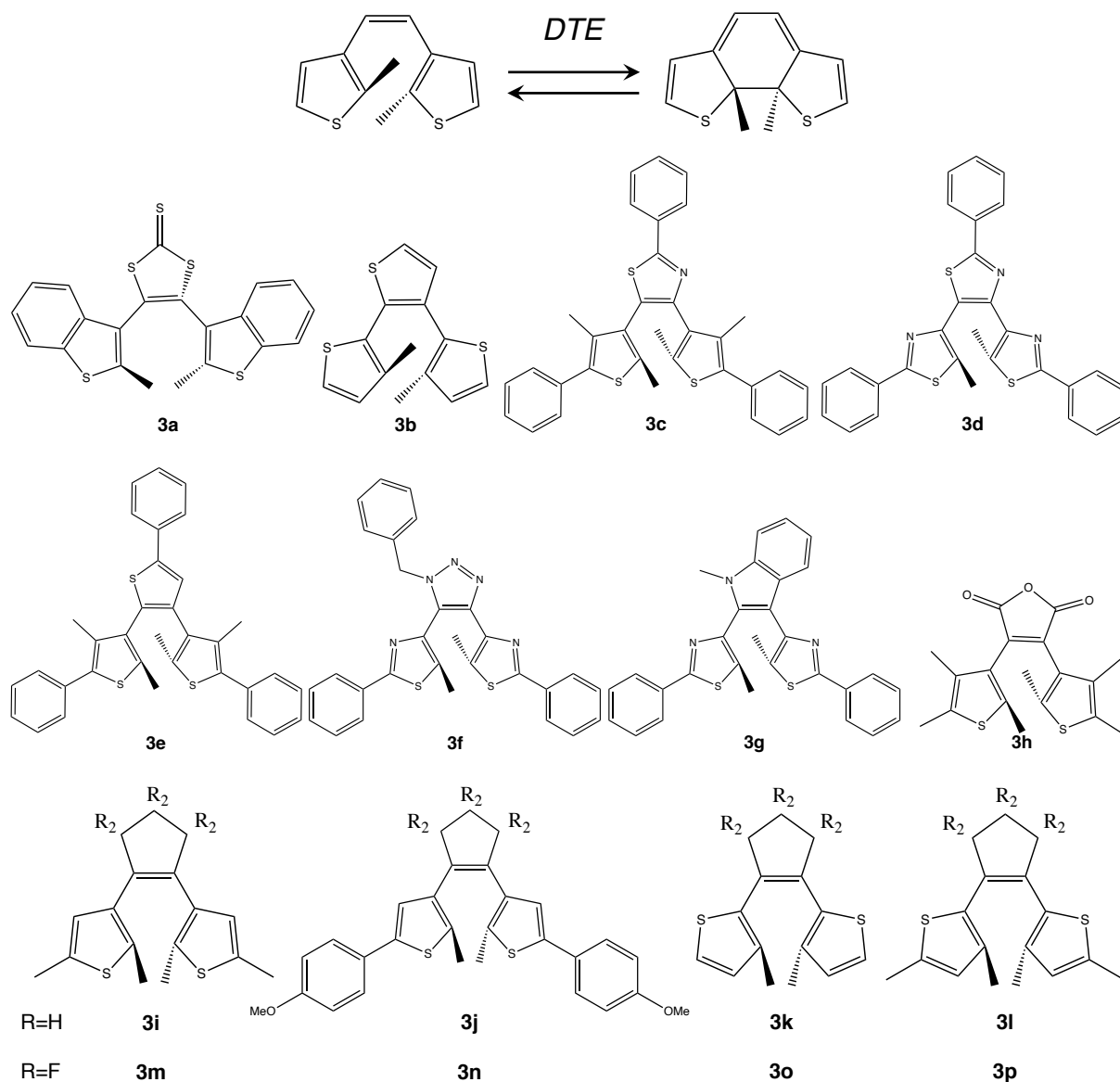


Figure 18. DTE compounds under study represented in their open form.

The set of DTE structures studied is presented in Figure 18. We have selected a wide range of structural motives to be representative of the diversity of compounds synthesized in the DTE family.⁵⁷ Because of the absence of parameters for fluor in the *mio* set of DFTB2 method, the fluorinated structures were limited to four systems, **3m-3p**, for which DFTB2 level could not be tested.

The mean errors and standard deviations of each structure calculated at the DLPNO-CCSD(T) level (E(CCSD(T)/OG(M))) with respect to the minimum energy structure

(E(CCSD(T)/MinG)) are presented in Figure 19. As for the other series, the methods leading to the lowest energy structures for both forms are B3LYP and r2SCAN-3c followed very closely by PBE. DFTB3(-D3) and XTB2 results are about 15 kJ/mol higher than the minimum energy structures. Interestingly, both forms (open and closed) show very similar errors which was not the case in the two first series. DFTB2(-D3) deviates strongly from the minima, resulting in energies of the open and closed form 30 kJ/mol and 20 kJ/mol higher than E(CCSD(T)/MinG) respectively. For the non-fluorinated systems, the largest errors for all TB methods are obtained for the systems containing a nitrogen in the central five-membered rings (**3d**, **3f** and **3g**), as it was noted also in the AZO series. For the fluorinated systems, DFTB3(-D3) performs worse than the rest of the tested systems with errors close to 30 kJ/mol for both forms. This underperformance is however not observed using XTB2.

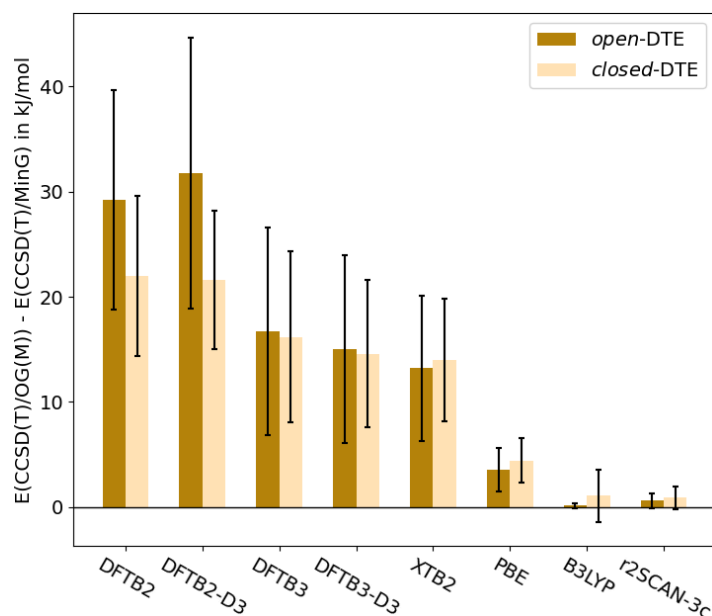


Figure 19. Mean error and standard deviation of E(CCSD(T)/OG(M)) with respect to E(CCSD(T)/MinG) for the DTE series.

Root mean square deviations (RMSD), mean bond length differences, difference in the distance between the two reacting carbon atoms (C-C), and errors on a dihedral angle (depicted in Figure 21) are shown in Figure 20. All TB methods show much larger RMSDs in the open form compared to the ones in the closed forms. The reactive C-C distances in the open form show much larger deviations than, especially for DFTB2(-D3) methods. On the other hand, the errors on the dihedral angle are much smaller for all TB methods in this series compared to the two previous ones. The closed DTE are obviously very rigid structures, but while rotation of the arms is possible for open isomers, the π conjugation of the core is enough to restrain dihedral

angles in this case. Overall, the mean bond length difference evolution follows the observation made on the mean errors observed for the energies apart from the PBE results, as previously noted in the NBD/QC series.

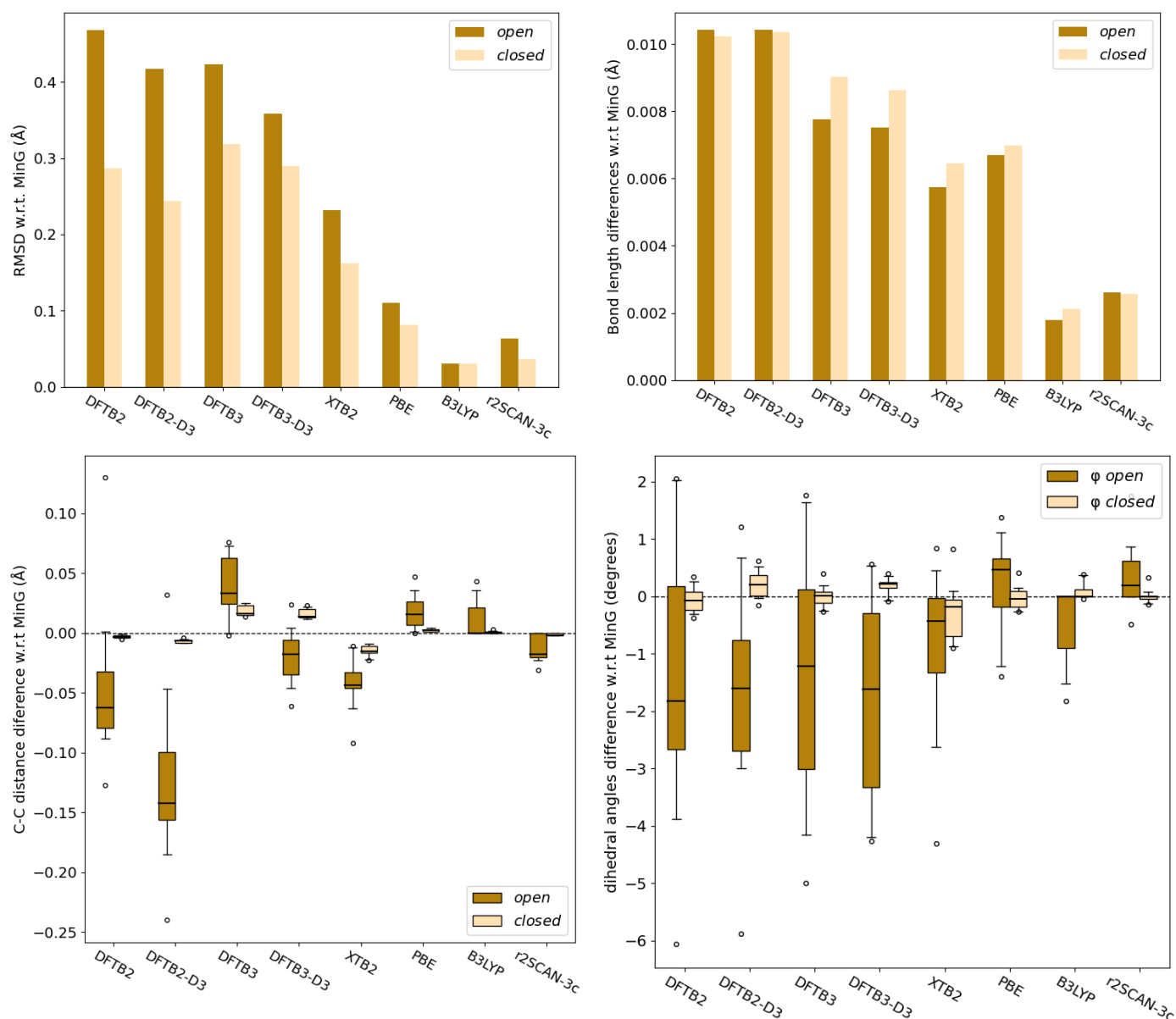


Figure 20. Top left: RMSD between each structure and the minimum energy structure (MinG). Top right: Mean bond length difference between each structure and MinG. Bottom left: difference in the distance between the two reacting carbon atoms (C-C) between each structure and MinG. Bottom right: dihedral angles difference between each structure and Min (see Figure 21 for details about the definition of the angle). See figure 4 for details about the boxplots.

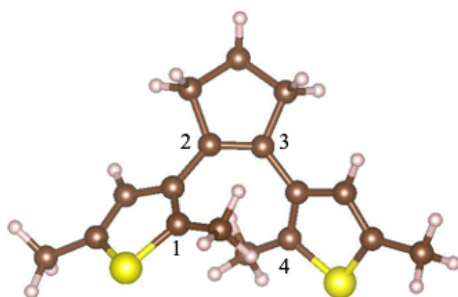


Figure 21. Illustration of the dihedral angle: φ corresponds to the dihedral angle between atoms 1,2,3 and 4.

The calculated $\Delta E(\text{CCSD(T)/MinG})$ values for the DTE series are reported in Figure 22 (right). The comparison of the calculated ΔE using each electronic structure methods (M) with respect to the ΔE calculated at the DLPNO-CCSD(T) level using either the structures obtained using method (M) for geometry optimization, or the minimum energy structure (MinG), is reported in Figure 22 (left). From $\Delta E(\text{M/OG(M)}) - \Delta E(\text{CCSD(T)/MinG})$, one can see that DFTB2(-D3) and DFTB3(-D3) perform very well and slightly outperforming PBE, B3LYP and r2SCAN-3c. This is particularly significant considering the diversity of the molecular structures in this set. The failure of XTB2 which largely underestimates ΔE appears clearly in this series. The very small errors obtained when calculating $\Delta E(\text{XTB2/OG(XTB2)}) - \Delta E(\text{CCSD(T)/OG(XTB2)})$ reveals that the error is not due to geometry optimizations but to the calculated energies. Indeed, the results of $\Delta E(\text{CCSD(T)/OG(XTB2)}) - \Delta E(\text{CCSD(T)/MinG})$ lead to results equivalent to those obtained at the DFTB3(-D3) levels and are better than the DFTB2(-D3) values. The D3 corrections moderately improve the DFTB2/DFTB3 results.

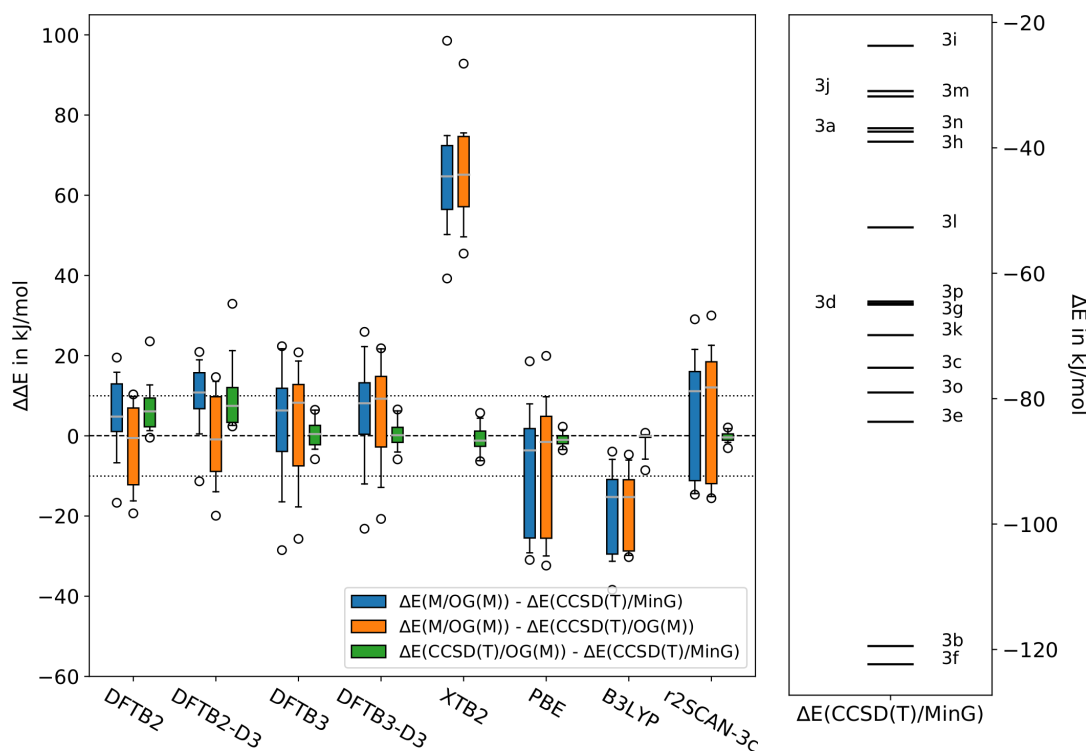


Figure 22. Left: Distribution of the errors of $\Delta E(\text{M}/\text{OG}(\text{M})) - \Delta E(\text{CCSD}(\text{T})/\text{MinG})$ in blue, $\Delta E(\text{M}/\text{OG}(\text{M})) - \Delta E(\text{CCSD}(\text{T})/\text{OG}(\text{M}))$ in orange and $\Delta E(\text{CCSD}(\text{T})/\text{OG}(\text{M})) - \Delta E(\text{CCSD}(\text{T})/\text{MinG})$ in green for the DTE series. See figure 4 for details about the boxplots. Right: $\Delta E(\text{CCSD}(\text{T})/\text{MinG})$ corresponding to the reference ΔE values.

DFTB2(-D3) and DFTB3(-D3) methods can be used alone to calculate ΔE values in the DTE series with a satisfying accuracy. As we just showed, this is not the case for the XTb2 method. However, geometries calculated at this level do provide very good results when the electronic structure is calculated at the DLPNO-CCSD(T) level. As for the other two series, $\Delta E(\text{PBE or r2SCAN-3c}/\text{OG}(\text{M})) - \Delta E(\text{PBE or r2SCAN-3c}/\text{OG}(\text{PBE or r2SCAN-3c}))$ and $\Delta E(\text{PBE or r2SCAN-3c}/\text{OG}(\text{M})) - \Delta E(\text{CCSD}(\text{T})/\text{MinG})$ for all TB methods as presented in Figure 23. Here, as DFTB2(-D3) and DFTB3(-D3) originally slightly outperform both PBE and r2SCAN-3c, this mixed approach leads to slightly larger errors than using these TB methods alone. However, it is still a reasonable approach when combined with XTb2 geometry optimization for both PBE and r2SCAN-3c with median errors within 10 kJ/mol.

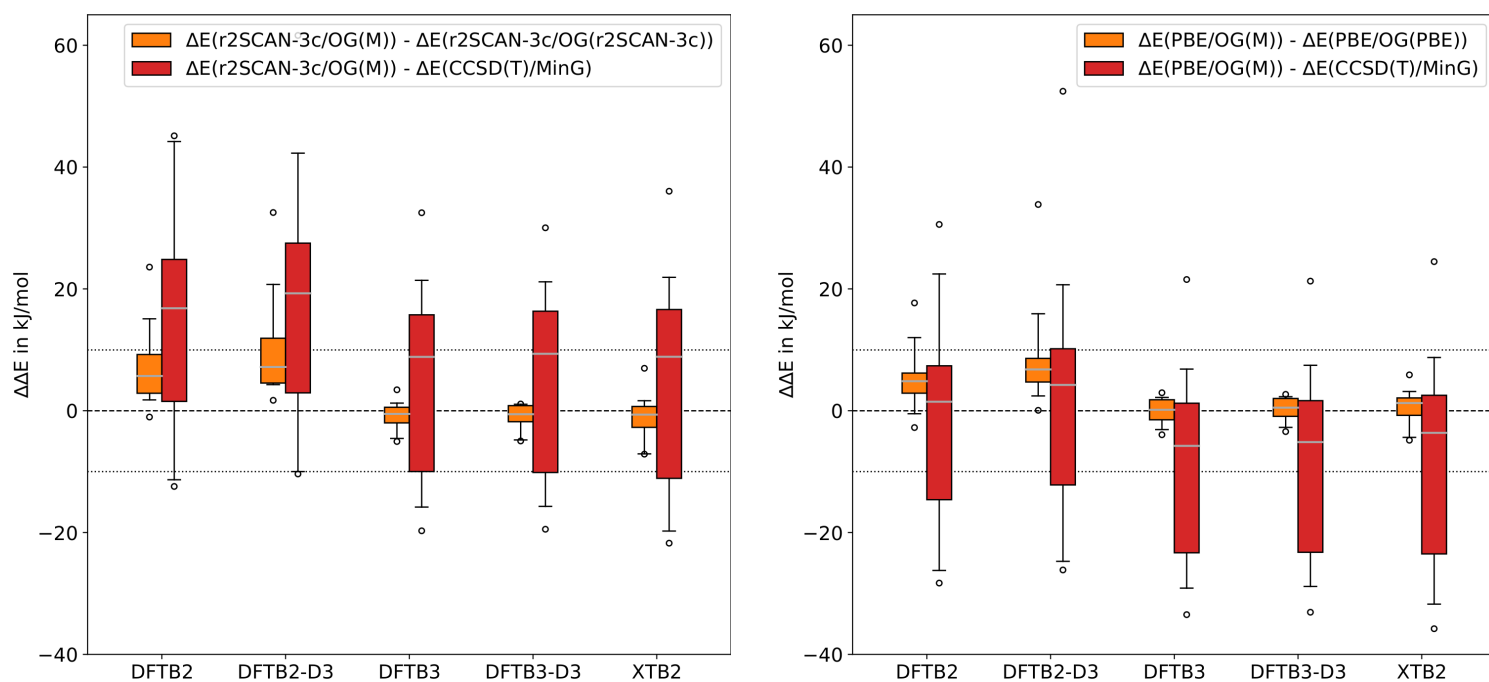


Figure 23. Left: Distribution of the errors of $\Delta E(\text{r2SCAN-3c/OG(M)}) - \Delta E(\text{r2SCAN-3c/OG(r2SCAN-3c)})$ and $\Delta E(\text{r2SCAN-3c/OG(M)}) - \Delta E(\text{CCSD(T)/MinG})$ for the DTE series. Right: Distribution of the errors of $\Delta E(\text{PBE/OG(M)}) - \Delta E(\text{PBE/OG(PBE)})$ and $\Delta E(\text{PBE/OG(M)}) - \Delta E(\text{CCSD(T)/MinG})$ for the DTE series. See figure 4 for details about the boxplots.

Energies and oscillator strengths of the first intense excited state computed at the TD-DFTB2, PBE, B3LYP, CAM-B3LYP and DLPNO-STEOM-CCSD levels for both isomers are given in Figure 24 (the first five excited states are compared in Figure S3). Note that LC-DFTB2 is excluded from this comparison as the parameters set does not contain a sulfur. The first electronic excitation is a $\pi\text{-}\pi^*$ HOMO-LUMO transition both in the closed and the open forms, for all DTE. As for the other series, CAM-B3LYP is the DFT functional leading to excited energies that are in average in best agreement with DLPNO-STEOM-CCSD as presented in Table 3. DFTB2 suffers from the same underestimation of the excited states energies as in the AZO and NBD/QC series.

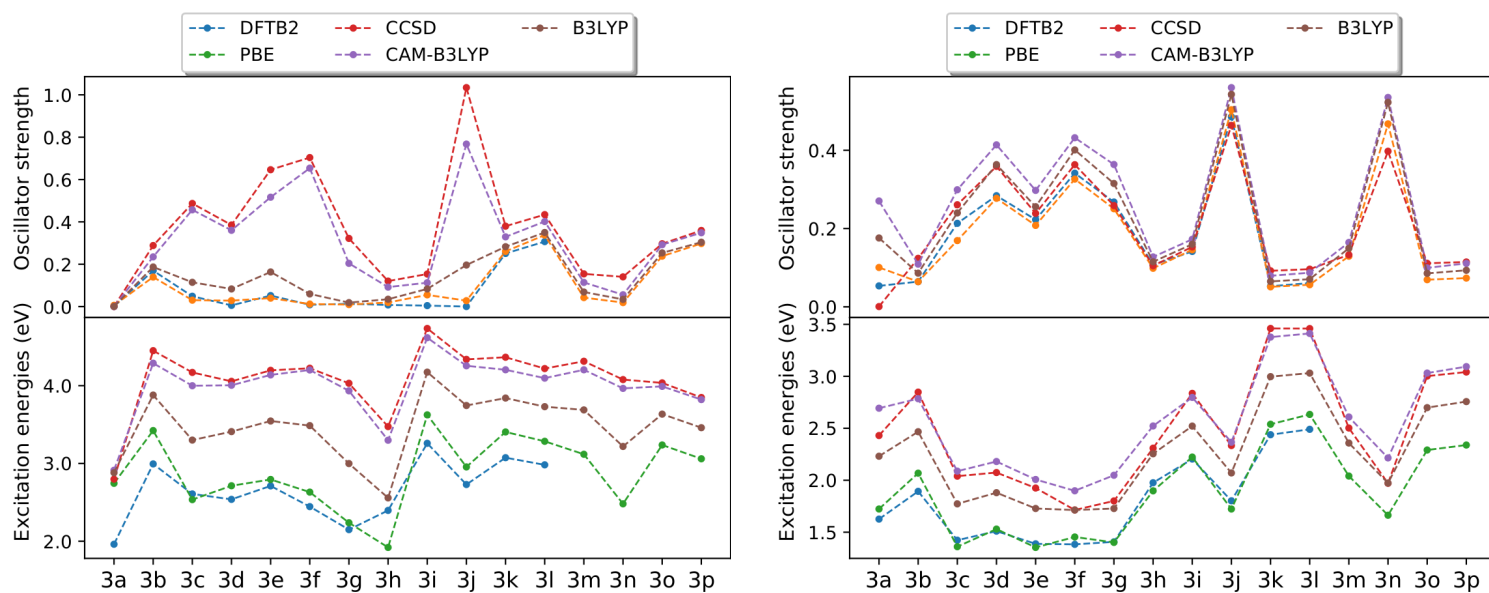


Figure 24. First intense singlet excited state energies and oscillator strength of the DTE series in the open (left) and closed (right) forms calculated using DFTB2, PBE, B3LYP, CAM-B3LYP, and STEOM-DLPNO-CCSD (see Methodology section for details).

Table 3. Mean absolute errors (eV) on the first maximum absorption (FMA) and oscillator strength with respect to STEOM-DLPNO-CCSD at the B3LYP geometries for the NBD/QC series.

	DFTB2		PBE		B3LYP		CAM-B3LYP	
	open	closed	open	closed	open	closed	open	closed
FMA	1.43	0.64	1.20	0.59	0.62	0.22	0.10	0.12
f	0.34	0.03	0.27	0.04	0.23	0.04	0.06	0.06

As an illustration of the performance of the different methods, we analyze in detail the simulated UV-visible spectra of the open and closed form of **3c** (Figure 25). The excited states description (principal monoexcitations, excitation energy and oscillator strength) as well as the relevant molecular orbitals are presented in Table S9 and S10, respectively. For both isomers, the natures of the frontier molecular orbitals are similar regardless of the level of calculation. However, for the open form, the transition from the HOMO to the first LUMOs levels lead to intense transitions at the B3LYP, CAM-B3LYP and DLPNO-STEOM-CCSD, while these transitions show low oscillator strengths with DFTB2 and PBE. For the two latter the largest oscillator strength is observed for an excitation from the HOMO-2 to the LUMO. For the closed form, the first peak corresponds in all cases to a HOMO to LUMO transition. The experimental first absorption maxima in hexane solution were found to be 4.6 eV for the open form and 2.0 eV for the closed form.⁵⁸ These experimental values are very close to the CAM-B3LYP and

DLPNO-STEOM-CCSD bands for both forms. Analysis of DFTB2 and PBE simulated spectra reveals a clear underestimation of the main peak maxima.

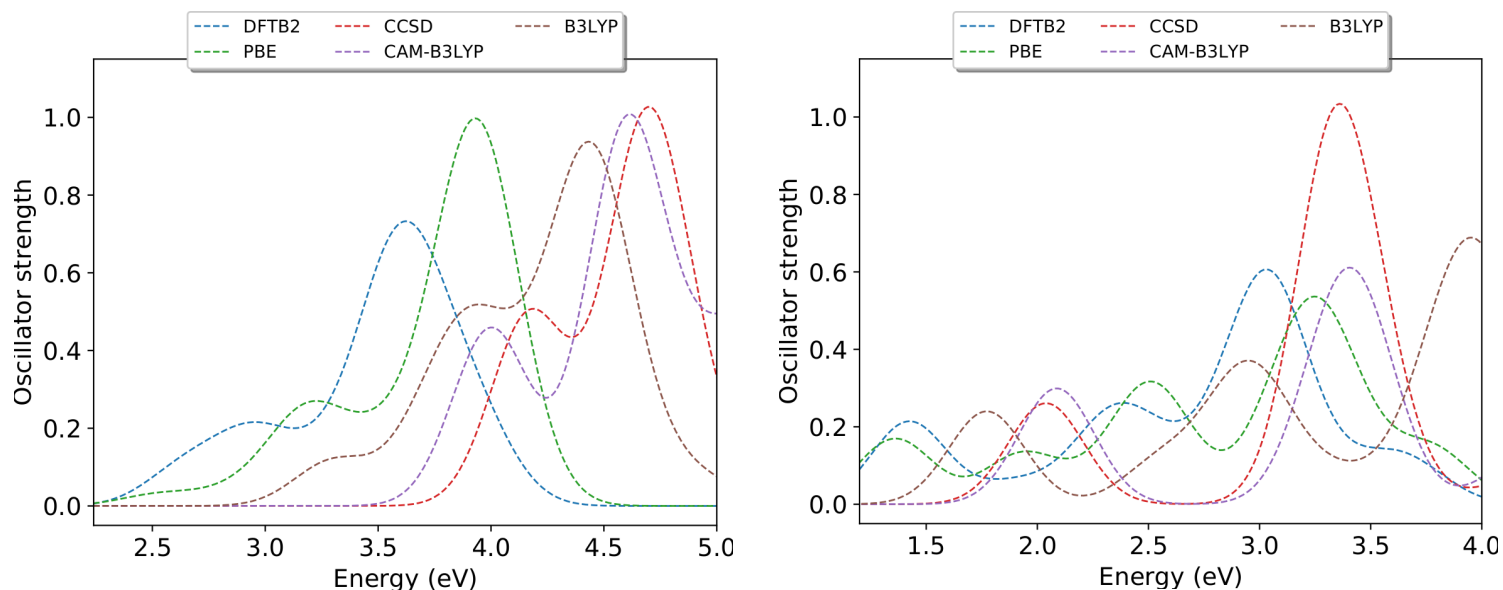


Figure 25. Simulated UV-Visible spectra of the open (left) and closed (right) forms of 3c calculated using DFTB2, PBE, B3LYP, CAM-B3LYP, and STEOM-DLPNO-CCSD (see Methodology section for details, convolution with gaussian functions with a full-width at half-maximum of 0.2 eV).

The accuracy of TB methods for the description of DTE photochromes can be summarized as follows:

- The best geometries are obtained with either DFTB3(-D3) or XTB2,
- DFTB2 and DFTB3 methods lead to very good estimations of ΔE , where XTB2 strongly underperforms,
- Single point calculations at DFT levels (PBE and r2SCAN-3c) using TB-optimized geometries lead to satisfying results but do not improve the full DFTB2 or DFTB3 calculations,
- In the absence of adapted LC-DFTB2 parameters, DFTB2 underestimates excitation energies similarly to a GGA DFT functional.

5 – Conclusion

Several key features were computed for three sets of photochromic organic molecules, namely azobenzene (AZO), norbornadiene/quadracyclane (NBD/QC) and diarylethene (DTE) derivatives, in order to investigate the accuracy of Tight-Binding (TB) DFT methods (DFTB2, DFTB3, XTB2, and LC-DFTB2 for excited states). We specifically focused our efforts on the

evaluation of the accuracy of the optimized geometries, the difference in energy between the two isomers of each photochroms (ΔE), and of the energies of the first relevant excited state. The results obtained when applying these TB semi-empirical methods were compared to those obtained at several DFT levels, namely PBE, B3LYP and r2SCAN-3c for the geometries and the ΔE and PBE, B3LYP and CAM-B3LYP for the excited states. The reference energy values used to assess the accuracy of the results are state-of-the-art electronic structure calculation methods, namely DLPNO-CCSD(T) for ground states and DLPNO-STEOM-CCSD for excited states.

In all cases, the inclusion of dispersion corrections (D3) at the DFTB2 or DFTB3 levels did not significantly improve the results. Overall, DFTB3 is the TB method leading to the best results for the geometries and the ΔE evaluation and can be use alone for these purposes for norbornadiene/quadracyclane and diarylethene derivatives. Single point calculations at the r2SCAN-3c level using TB geometries is a good solution to circumvent the deficiencies of these semi-empirical methods in the azobenzene series. For the description of electronic transitions, the range-separated LC-DFTB2 method is the most consistent and accurate, providing UV-visible spectra of azobenzene derivatives in close agreement with the reference. While overestimating the transition energies for the norbornadiene/quadracyclane derivatives this method still outperforms its non-range-separated version (DFTB2) for this series. The limitation of this method is mostly the lack parameters for a wide range of atoms, and the presence of sulfur in the DTE core limit the TB description to the use of DFTB2 that underestimates non-negligibly the transitions energies. For a more extensive comparative study of these photoreactive molecules, the present work shall be extended to include the characterization of transition-states and energy barriers.

Through the evaluation of the performances of the very computationally efficient semi-empirical TB models (calculation times are in the order of a few seconds on a standard personal computer), this comparative works paves the way towards a more systematic use of such methods for the study of photochromic material, that will allow to increase significantly either the number of atoms explicitly present in the simulation or the time scale of the events to be tackled (dynamic effects) thus providing new ways of conducting computer-assisted design of photo-responsive material.

Supplementary material

See supplementary material for data on ΔE values and on the first five excited states of each series of compounds. Additionally, details about the nature of the electronic transitions of the example molecule for each series are presented.

Acknowledgements

This work was supported by the ANR FALCON project, grant ANR-20-CE09-0002-01, of the French Agence Nationale de la Recherche. Calculations were performed at ISCR and the work was granted access by the French GENCI agency for HPC resources of TGCC/CINES/IDRIS under the allocation A0100800649 and AD010800649R1. The authors thank Rémi Marchal for technical support on the local calculation server.

Authors declarations

The authors declare that they have no known competing financial interests or personal relationships that could have appeared to influence the work reported in this paper.

References

- (1) Saydjari, A. K.; Weis, P.; Wu, S.; Saydjari, A. K.; Weis, P.; Wu, S. Spanning the Solar Spectrum: Azopolymer Solar Thermal Fuels for Simultaneous UV and Visible Light Storage. *Adv. Energy Mater.* **2017**, *7* (3), 1601622. <https://doi.org/10.1002/AENM.201601622>.
- (2) Wang, Z.; Erhart, P.; Li, T.; Zhang, Z. Y.; Sampedro, D.; Hu, Z.; Wegner, H. A.; Brummel, O.; Libuda, J.; Nielsen, M. B.; Moth-Poulsen, K. Storing Energy with Molecular Photoisomers. *Joule* **2021**, *5* (12), 3116–3136. <https://doi.org/10.1016/j.joule.2021.11.001>.
- (3) Feng, Y.; Liu, H.; Luo, W.; Liu, E.; Zhao, N.; Yoshino, K.; Feng, W. Covalent Functionalization of Graphene by Azobenzene with Molecular Hydrogen Bonds for Long-Term Solar Thermal Storage. *Sci. Reports* **2013**, *3* (1), 1–8. <https://doi.org/10.1038/srep03260>.
- (4) Zhitomirsky, D.; Cho, E.; Grossman, J. C.; Zhitomirsky, D.; Cho, E.; Grossman, J. C. Solid-State Solar Thermal Fuels for Heat Release Applications. *Adv. Energy Mater.* **2016**, *6* (6), 1502006. <https://doi.org/10.1002/AENM.201502006>.
- (5) Kucharski, T. J.; Ferralis, N.; Kolpak, A. M.; Zheng, J. O.; Nocera, D. G.; Grossman, J. C. Templated Assembly of Photoswitches Significantly Increases the Energy-Storage Capacity of Solar Thermal Fuels. *Nat. Chem.* **2014**, *6* (5), 441–447.

<https://doi.org/10.1038/nchem.1918>.

- (6) Russew, M. M.; Hecht, S. Photoswitches: From Molecules to Materials. *Adv. Mater.* **2010**, *22* (31), 3348–3360. <https://doi.org/10.1002/ADMA.200904102>.
- (7) Szymański, W.; Beierle, J. M.; Kistemaker, H. A. V.; Velema, W. A.; Feringa, B. L. Reversible Photocontrol of Biological Systems by the Incorporation of Molecular Photoswitches. *Chem. Rev.* **2013**, *113* (8), 6114–6178. https://doi.org/10.1021/CR300179F/ASSET/IMAGES/CR300179F.SOCIAL.JPEG_V03.
- (8) Bléger, D.; Hecht, S. Visible-Light-Activated Molecular Switches. *Angew. Chemie Int. Ed.* **2015**, *54* (39), 11338–11349. <https://doi.org/10.1002/ANIE.201500628>.
- (9) Göstl, R.; Senf, A.; Hecht, S. Remote-Controlling Chemical Reactions by Light: Towards Chemistry with High Spatio-Temporal Resolution. *Chem. Soc. Rev.* **2014**, *43* (6), 1982–1996. <https://doi.org/10.1039/C3CS60383K>.
- (10) Fihey, A.; Russo, R.; Cupellini, L.; Jacquemin, D.; Mennucci, B. Is Energy Transfer Limiting Multiphotochromism? Answers from Ab Initio Quantifications. *Phys. Chem. Chem. Phys.* **2017**, *19* (3), 2044–2052. <https://doi.org/10.1039/C6CP07458H>.
- (11) Gur, I.; Sawyer, K.; Prasher, R. Searching for a Better Thermal Battery. *Science* (80-.). **2012**, *335* (6075), 1454–1455. <https://doi.org/10.1126/SCIENCE.1218761>.
- (12) Bandara, H. M. D.; Burdette, S. C. Photoisomerization in Different Classes of Azobenzene. *Chem. Soc. Rev.* **2012**, *41* (5), 1809–1825. <https://doi.org/10.1039/C1CS15179G>.
- (13) Klajn, R. Spiropyran-Based Dynamic Materials. *Chem. Soc. Rev.* **2013**, *43* (1), 148–184. <https://doi.org/10.1039/C3CS60181A>.
- (14) Irie, M.; Fukaminato, T.; Matsuda, K.; Kobatake, S. Photochromism of Diarylethene Molecules and Crystals: Memories, Switches, and Actuators. **2014**. <https://doi.org/10.1021/cr500249p>.
- (15) Orrego-Hernández, J.; Dreos, A.; Moth-Poulsen, K. Engineering of Norbornadiene/Quadricyclane Photoswitches for Molecular Solar Thermal Energy Storage Applications. *Acc. Chem. Res.* **2020**, *53* (8), 1478–1487. <https://doi.org/10.1021/acs.accounts.0c00235>.
- (16) Pijper, T. C.; Ivashenko, O.; Walko, M.; Rudolf, P.; Browne, W. R.; Feringa, B. L. Position and Orientation Control of a Photo- and Electrochromic Dithienylethene Using a Tripodal Anchor on Gold Surfaces. **2015**. <https://doi.org/10.1021/jp512424d>.
- (17) Schuschke, C.; Hohner, C.; Jevric, M.; Ugleholdt Petersen, A.; Wang, Z.; Schwarz, M.;

- Kettner, M.; Waidhas, F.; Fromm, L.; Sumbly, C. J.; Görling, A.; Brummel, O.; Moth-Poulsen, K.; Libuda, J. Solar Energy Storage at an Atomically Defined Organic-Oxide Hybrid Interface. *Nat. Commun.* **2019**, *10* (1), 1–10. <https://doi.org/10.1038/s41467-019-10263-4>.
- (18) Elstner, M.; Porezag, D.; Jungnickel, G.; Elsner, J.; Haugk, M.; Frauenheim, T.; Suhai, S.; Seifert, G. Self-Consistent-Charge Density-Functional Tight-Binding Method for Simulations of Complex Materials Properties. *Phys. Rev. B* **1998**, *58* (11), 7260. <https://doi.org/10.1103/PhysRevB.58.7260>.
- (19) Gaus, M.; Cui, Q.; Elstner, M. DFTB3: Extension of the Self-Consistent-Charge Density-Functional Tight-Binding Method (SCC-DFTB). *J. Chem. Theory Comput.* **2011**, *7* (4), 931–948. <https://doi.org/10.1021/CT100684S>.
- (20) Bannwarth, C.; Ehlert, S.; Grimme, S. GFN2-XTB—An Accurate and Broadly Parametrized Self-Consistent Tight-Binding Quantum Chemical Method with Multipole Electrostatics and Density-Dependent Dispersion Contributions. *J. Chem. Theory Comput.* **2019**, *15* (3), 1652–1671. <https://doi.org/10.1021/ACS.JCTC.8B01176>.
- (21) Spiegelman, F.; Tarrat, N.; Cuny, J.; Dontot, L.; Posenitskiy, E.; Martí, C.; Simon, A.; Rapacioli, M. Density-Functional Tight-Binding: Basic Concepts and Applications to Molecules and Clusters. <https://doi-org.passerelle.univ-rennes1.fr/10.1080/23746149.2019.1710252> **2020**, *5* (1), 1710252. <https://doi.org/10.1080/23746149.2019.1710252>.
- (22) Uratani, H.; Yoshikawa, T.; Nakai, H. Trajectory Surface Hopping Approach to Condensed-Phase Nonradiative Relaxation Dynamics Using Divide-and-Conquer Spin-Flip Time-Dependent Density-Functional Tight Binding. *J. Chem. Theory Comput.* **2021**, *17* (3), 1290–1300. <https://doi.org/10.1021/acs.jctc.0c01155>.
- (23) Do Varella, M. T. N.; Stojanovic, L.; Vuong, V. Q.; Irle, S.; Niehaus, T. A.; Barbatti, M. How the Size and Density of Charge-Transfer Excitons Depend on Heterojunction's Architecture. *J. Phys. Chem. C* **2021**, *125* (10), 5458–5474. https://doi.org/10.1021/ACS.JPCC.0C10762/SUPPL_FILE/JP0C10762_SI_002.ZIP.
- (24) Koerstz, M.; Christensen, A. S.; Mikkelsen, K. V.; Nielsen, M. B.; Jensen, J. H. High Throughput Virtual Screening of 230 Billion Molecular Solar Heat Battery Candidates. *PeerJ Phys. Chem.* **2021**, *3*, e16. <https://doi.org/10.7717/PEERJ-PCHEM.16>.
- (25) Szabo, R.; Le, K. N.; Kowalczyk, T. Multifactor Theoretical Modeling of Solar Thermal Fuels Built on Azobenzene and Norbornadiene Scaffolds. *Sustain. Energy Fuels* **2021**, *5* (8), 2335–2346. <https://doi.org/10.1039/d1se00041a>.

- (26) Dong, L.; Feng, Y.; Wang, L.; Feng, W. Azobenzene-Based Solar Thermal Fuels: Design, Properties, and Applications. *Chem. Soc. Rev.* **2018**, *47* (19), 7339–7368. <https://doi.org/10.1039/c8cs00470f>.
- (27) Quant, M.; Lennartson, A.; Dreos, A.; Kuisma, M.; Erhart, P.; Börjesson, K.; Moth-Poulsen, K. Low Molecular Weight Norbornadiene Derivatives for Molecular Solar-Thermal Energy Storage. *Chem. - A Eur. J.* **2016**, *22* (37), 13265–13274. <https://doi.org/10.1002/chem.201602530>.
- (28) Jevric, M.; Petersen, A. U.; Mansø, M.; Kumar Singh, S.; Wang, Z.; Dreos, A.; Sumbly, C.; Nielsen, M. B.; Börjesson, K.; Erhart, P.; Moth-Poulsen, K. Norbornadiene-Based Photoswitches with Exceptional Combination of Solar Spectrum Match and Long-Term Energy Storage. *Chem. - A Eur. J.* **2018**, *24* (49), 12767–12772. <https://doi.org/10.1002/chem.201802932>.
- (29) Vuong, V. Q.; Jissy, #; Kuriappan, A.; Kubillus, M.; Kranz, J. J.; Mast, T.; Niehaus, T. A.; Irle, S.; Elstner, M. Parametrization and Benchmark of Long-Range Corrected DFTB2 for Organic Molecules. **2017**. <https://doi.org/10.1021/acs.jctc.7b00947>.
- (30) Grimme, S.; Ehrlich, S.; Goerigk, L. Effect of the Damping Function in Dispersion Corrected Density Functional Theory. *J. Comput. Chem.* **2011**, *32* (7), 1456–1465. <https://doi.org/10.1002/jcc.21759>.
- (31) Perdew, J. P.; Burke, K.; Ernzerhof, M. Generalized Gradient Approximation Made Simple. *Phys. Rev. Lett.* **1996**, *77* (18), 3865–3868. <https://doi.org/10.1103/PhysRevLett.77.3865>.
- (32) Becke, A. D. Density-functional Thermochemistry. III. The Role of Exact Exchange. *J. Chem. Phys.* **1993**, *98* (7), 5648–5652. <https://doi.org/10.1063/1.464913>.
- (33) Yanai, T.; Tew, D. P.; Handy, N. C. A New Hybrid Exchange-Correlation Functional Using the Coulomb-Attenuating Method (CAM-B3LYP). *Chem. Phys. Lett.* **2004**, *393* (1–3), 51–57. <https://doi.org/10.1016/j.cplett.2004.06.011>.
- (34) Grimme, S.; Hansen, A.; Ehlert, S.; Mewes, J.-M. R2SCAN-3c: A “Swiss Army Knife” Composite Electronic-Structure Method. *J. Chem. Phys.* **2021**, *154* (6), 064103. <https://doi.org/10.1063/5.0040021>.
- (35) Riplinger, C.; Sandhoefer, B.; Hansen, A.; Neese, F. Natural Triple Excitations in Local Coupled Cluster Calculations with Pair Natural Orbitals. *J. Chem. Phys.* **2013**, *139* (13), 134101. <https://doi.org/10.1063/1.4821834>.
- (36) Liakos, D. G.; Guo, Y.; Neese, F. Comprehensive Benchmark Results for the Domain Based Local Pair Natural Orbital Coupled Cluster Method (DLPNO-CCSD(T)) for

- Closed- and Open-Shell Systems. *J. Phys. Chem. A* **2019**, *124* (1), 90–100. <https://doi.org/10.1021/ACS.JPCA.9B05734>.
- (37) Kabsch, W. A Solution for the Best Rotation to Relate Two Sets of Vectors. *Acta Crystallogr. Sect. A* **1976**, *32* (5), 922–923. <https://doi.org/10.1107/S0567739476001873>.
- (38) Walker, M. W.; Shao, L.; Volz, R. A. Estimating 3-D Location Parameters Using Dual Number Quaternions. *CVGIP Image Underst.* **1991**, *54* (3), 358–367. [https://doi.org/10.1016/1049-9660\(91\)90036-O](https://doi.org/10.1016/1049-9660(91)90036-O).
- (39) Niehaus, T. A.; Suhai, S.; Sala, F. Della; Lugli, P.; Elstner, M.; Seifert, G.; Frauenheim, T. Tight-Binding Approach to Time-Dependent Density-Functional Response Theory. <https://doi.org/10.1103/PhysRevB.63.085108>.
- (40) Nooijen, M.; Bartlett, R. J. A New Method for Excited States: Similarity Transformed Equation-of-Motion Coupled-Cluster Theory. *J. Chem. Phys.* **1998**, *106* (15), 6441. <https://doi.org/10.1063/1.474000>.
- (41) Nooijen, M.; Bartlett, R. J. Similarity Transformed Equation-of-Motion Coupled-Cluster Theory: Details, Examples, and Comparisons. *J. Chem. Phys.* **1998**, *107* (17), 6812. <https://doi.org/10.1063/1.474922>.
- (42) Dutta, A. K.; Nooijen, M.; Neese, F.; Izsák, R. Automatic Active Space Selection for the Similarity Transformed Equations of Motion Coupled Cluster Method. *J. Chem. Phys.* **2017**, *146* (7), 074103. <https://doi.org/10.1063/1.4976130>.
- (43) Dutta, A. K.; Nooijen, M.; Neese, F.; Izsák, R. Exploring the Accuracy of a Low Scaling Similarity Transformed Equation of Motion Method for Vertical Excitation Energies. *J. Chem. Theory Comput.* **2018**, *14* (1), 72–91. https://doi.org/10.1021/ACS.JCTC.7B00802/SUPPL_FILE/CT7B00802_SI_001.PDF.
- (44) Neese, F.; Wennmohs, F.; Becker, U. The ORCA Quantum Chemistry Program Package. *J. Chem. Phys.* **2020**, *152*, 224108. <https://doi.org/10.1063/5.0004608>.
- (45) Hourahine, B.; Aradi, B.; Blum, V.; Bonafé, F.; Buccheri, A.; Camacho, C.; Cevallos, C.; Deshayé, M. Y.; Dumitrică, T.; Dominguez, A.; Ehlert, S.; Elstner, M.; Heide, T. van der; Hermann, J.; Irlé, S.; Kranz, J. J.; Köhler, C.; Kowalczyk, T.; Kubař, T.; Lee, I. S.; Lutsker, V.; Maurer, R. J.; Min, S. K.; Mitchell, I.; Negre, C.; Niehaus, T. A.; Niklasson, A. M. N.; Page, A. J.; Pecchia, A.; Penazzi, G.; Persson, M. P.; Řezáč, J.; Sánchez, C. G.; Sternberg, M.; Stöhr, M.; Stuckenberg, F.; Tkatchenko, A.; Yu, V. W. -z.; Frauenheim, T. DFTB+, a Software Package for Efficient Approximate Density Functional Theory Based Atomistic Simulations. *J. Chem. Phys.* **2020**, *152* (12), 124101.

<https://doi.org/10.1063/1.5143190>.

- (46) Weigend, F.; Ahlrichs, R. Balanced Basis Sets of Split Valence, Triple Zeta Valence and Quadruple Zeta Valence Quality for H to Rn: Design and Assessment of Accuracy. *Phys. Chem. Chem. Phys.* **2005**, *7* (18), 3297–3305. <https://doi.org/10.1039/B508541A>.
- (47) Kendall, R. A.; Früchtl, H. A. The Impact of the Resolution of the Identity Approximate Integral Method on Modern Ab Initio Algorithm Development. *Theor. Chem. Acc.* **1997**, *97* (1–4), 158–163. <https://doi.org/10.1007/s002140050249>.
- (48) Neese, F.; Wennmohs, F.; Hansen, A.; Becker, U. Efficient, Approximate and Parallel Hartree–Fock and Hybrid DFT Calculations. A ‘Chain-of-Spheres’ Algorithm for the Hartree–Fock Exchange. *Chem. Phys.* **2009**, *356* (1), 98–109. <https://doi.org/10.1016/j.chemphys.2008.10.036>.
- (49) Jr., T. H. D. Gaussian Basis Sets for Use in Correlated Molecular Calculations. I. The Atoms Boron through Neon and Hydrogen. *J. Chem. Phys.* **1998**, *90* (2), 1007. <https://doi.org/10.1063/1.456153>.
- (50) Woon, D. E.; Jr., T. H. D. Calculation of the Electron Affinities of the Second Row Atoms: Al–Cl. *J. Chem. Phys.* **1998**, *99* (5), 3730. <https://doi.org/10.1063/1.466148>.
- (51) Liakos, D. G.; Sparta, M.; Kesharwani, M. K.; Martin, J. M. L.; Neese, F. Exploring the Accuracy Limits of Local Pair Natural Orbital Coupled-Cluster Theory. *J. Chem. Theory Comput.* **2015**, *11* (4), 1525–1539. <https://doi.org/10.1021/CT501129S>.
- (52) Olmsted, J.; Lawrence, J.; Yee, G. G. Photochemical Storage Potential of Azobenzenes. *Sol. Energy* **1983**, *30* (3), 271–274. [https://doi.org/10.1016/0038-092X\(83\)90156-1](https://doi.org/10.1016/0038-092X(83)90156-1).
- (53) Weston, C. E.; Richardson, R. D.; Haycock, P. R.; White, A. J. P.; Fuchter, M. J. Arylazopyrazoles: Azoheteroarene Photoswitches Offering Quantitative Isomerization and Long Thermal Half-Lives. *J. Am. Chem. Soc.* **2014**, *136* (34), 11878–11881. <https://doi.org/10.1021/ja505444d>.
- (54) Beharry, A. A.; Sadovski, O.; Woolley, G. A. Azobenzene Photoswitching without Ultraviolet Light. *J. Am. Chem. Soc.* **2011**, *133* (49), 19684–19687. <https://doi.org/10.1021/ja209239m>.
- (55) Humeniuk, A.; Mitrić, R. Long-Range Correction for Tight-Binding TD-DFT. *J. Chem. Phys.* **2015**, *143* (13). <https://doi.org/10.1063/1.4931179>.
- (56) Vetráková, E.; Ladányi, V.; Al Anshori, J.; Dvořák, P.; Wirz, J.; Heger, D. The Absorption Spectrum of Cis-Azobenzene †. *Photochem. Photobiol. Sci.* **2017**, *16*, 1749. <https://doi.org/10.1039/c7pp00314e>.
- (57) Irie, M.; Fukaminato, T.; Matsuda, K.; Kobatake, S. Photochromism of Diarylethene

Molecules and Crystals: Memories, Switches, and Actuators. *Chem. Rev.* **2014**, *114* (24), 12174–12277. <https://doi.org/10.1021/CR500249P>.

- (58) Nakashima, T.; Atsumi, K.; Kawai, S.; Nakagawa, T.; Hasegawa, Y.; Kawai, T. Photochromism of Thiazole-Containing Triangle Terarylenes. *European J. Org. Chem.* **2007**, *2007* (19), 3212–3218. <https://doi.org/10.1002/ejoc.200700074>.